INTRA-OPERATIVE REGISTRATION METHODS

FOR IMAGE-GUIDED KIDNEY SURGERY

By

Rowena E. Ong

Dissertation

Submitted to the Faculty of the

Graduate School of Vanderbilt University

in partial fulfillment of the requirements

for the degree of

DOCTOR OF PHILOSOPHY

in

Biomedical Engineering

May, 2012

Nashville, Tennessee

Approved:

Dr. Robert L. Galloway

Dr. Michael I. Miga

Dr. S. Duke Herrell

Dr. Benoit Dawant

Dr. Robert J. Webster, III

ACKNOWLEDGEMENTS

TABLE OF CONTENTS

LIST OF FIGURES

Figure

LIST OF TABLES

LIST OF ABBREVIATIONS

Abbreviation	Full Name
1. CT	Computed tomography
2. FRE	Fiducial registration error
3. IACUC	Institutional Animal Care and Use Committee
4. ICP	Iterative Closest Point
5. keV	kilo-electron volt
6. LRS	Laser range scanner
7. mAs	milliampere-second
8. MIS	Minimally invasive surgery
9. MR	Magnetic resonance
10. TPS	Thin-plate spline
11. TRE	Target registration error

CHAPTER 1

INTRODUCTION

The American Cancer Society has estimated that over 54,000 new cases of renal cancer will be diagnosed and over 13,000 people will die of the disease in 2008 [1]. Surgery is the commonly recommended treatment if the renal tumors are found prior to metastasis. Partial nephrectomies, in which only a portion of the kidney is removed, are usually recommended instead of full nephrectomies for small renal tumors. Recent studies [2-3] have found that patients who undergo partial nephrectomies have about the same tumor re-occurrence and long-term survival rates as those who undergo radical nephrectomies; however, partial nephrectomy patients have the advantage of retaining greater renal function.

In performing partial nephrectomies, surgeons have increasingly been using minimally invasive approaches. In minimally invasive surgery (MIS), smaller incisions are used, and specially made surgical tools and a laparoscopic or endoscopic video camera with lighting are inserted. The surgery is performed by viewing the affected area and tools through the video. In abdominal laproscopy, the abdomen is insufflated with gas, usually carbon dioxide, to create enough space around the organ to perform the surgery. Because of the smaller incisions made and the healthy tissue saved, minimally invasive surgeries have been shown to result in faster recovery times and reduced scarring compared to open procedures [4-5]. However, the challenges in terms of surgical dexterity, visualization and orientation in an unevenly-illuminated cavity, and the manipulation of multiple tools in a small space can make minimally invasive surgery difficult. Laparoscopy's widespread usage has been facilitated by robotics, which allow for finer control of tools through small ports [6-7].

Incorporating image guidance into minimally invasive partial nephrectomies could provide further benefits by allowing surgeons to more easily orient themselves, visualize tumor margins, and avoid critical healthy structures such as vessels. Image guidance provides a navigational aid for the surgeon by displaying the patient's target anatomy, usually obtained from pre- or intra-operative imaging, aligned with the current location of the surgical instruments. Image guidance systems track the locations of the moving surgical instruments

relative to the patient's physical body. In the surgical navigation parlance, the coordinate system used to record the locations of the tracked instruments and the patient's physical body is called the *physical space*. The coordinate system used in the patient's pre- or intra-operative image is called the *image space*. Image guided surgery systems use a *registration* method to align the physical space to the image space.

Registration is a method which transforms one coordinate space into another. Registration in a very general sense could align image-to-image, image-to-physical, or physical-to-physical space, and the transformations between spaces could be rigid, affine, or non-linear. There are two main types of registration methods: intensity-based and feature-based. Intensity-based registration methods use the intensities in the medical images to align two coordinate spaces. Feature-based methods could be point-based [8], surface-based [9], or use other features derived from either image or physical space for registration.

Previous work in image guidance has shown promising results, and image guidance is currently commercially available for applications such as cranial, ENT, orthopedic, and liver procedures (Medtronic Navigation, Louisville, CO; BrainLab, Feldkirchen, Germany; Pathfinder Therapeutics, Nashville, TN).

Different imaging modalities such as computed tomography (CT), bi-planar fluoroscopy, 3D fluoroscopy, magnetic resonance (MR), ultrasound, and laparoscopic /endoscopic video have been used in image guided systems. These imaging modalities can be used pre-operatively (before the surgery) or intra-operatively (during the surgery). Generally, image guided surgery systems use a high quality pre-operative CT or MR image, which is then registered to a tracked intra-operative images or data.

However, each of these imaging modalities has its limitations: ultrasound has limited imaging capabilities, signal to noise, and presents measurement challenges due to velocity changes through tissue; laparoscopic camera and fluoroscopy provide only 2D images which can be difficult to use for navigation; CT and 3D fluoroscopy involve radiation exposure to patient and surgeon; finally, intraoperative MR requires an MR-compatible operating suite and has cost problems as well as patient access challenges [10, 11].

One promising method uses a laser range scanner (LRS) to collect intra-operative data useful for navigation. It has successfully been used in liver and brain registrations [12-14]. However, a clinical study evaluating the use of the LRS for intra-operative guidance in the kidney had not been performed.

Therefore, the first goal of this work was to evaluate the use of the LRS for intra-operative registration in clinical open (i.e. large incision) partial nephrectomies. Chapter 2 presents the feasibility of a registration method to account for intra-operative kidney movement using texture-mapped LRS scans.

While laser range scanning is a promising method for intra-operative registration, it cannot be currently used for minimally invasive surgery. The current LRS system used is too large to fit into the laparoscopic trocar ports, and the triangulation method used to calculate distances makes it difficult to design a system small enough to fit through one port.

To address this issue, the second goal of this work (Chapters 3 and 4) was to explore conoscopic holography for intra-operative registration in minimally invasive surgeries. Conoscopic holography is a method for measuring the distance to an object at a single point using a reflected laser beam. In this method, the reflected light is passed through a polarizer and crystal, and the resulting phase changes and interference pattern can be used to calculate the distance to the object [15-16]. Unlike the LRS, which uses a stereoscopic method to calculate distance, the conoscopic laser can be made small enough to fit through a trocar port. When optically tracked, the conoscopic can be swept across an organ surface to obtain a 3D point cloud. An accuracy study of the geometric surface obtained by an optically-tracked conoscope can be found in [17], registration accuracy studies have been performed [18], and a clinical application for brain tumor resection has been evaluated [19].

Although these results are promising, the conoscope only gives a point cloud for use in surface-based registration. While this is useful for registration in some applications, the kidney's smooth, uniform shape and lack of distinctive geometric features may limit the accuracy of a pure surface-based registration. To remedy this problem, this work presents a novel method of texture-mapping the conoscopic surface using a laparoscopic camera. The

purpose of obtaining the texture map is to track texture features, natural or artificial, to aid in the registration of the kidney during gross movement or deformation in surgery.

Therefore, in chapter 3, a novel method is presented to texture-mapping a conoscopic surface using a laparoscopic camera. The calibration and accuracy of the method were investigated using ex-vivo porcine and human cadaver kidneys.

In chapter 4, the feasibility of the intra-operative registration method using the textured conoscopic surfaces is shown in-vivo, laparoscopic conditions. While this paper focuses on kidney applications, this method could be applied to other abdominal organs such as the liver.

Finally, the third goal of this work was to perform a preliminary study of the non-rigid deformation experienced by the kidney during surgery. While there have been studies examining the stiffness of the ex-vivo kidney in swine [20-21], the deformation of the human kidney during partial nephrectomies is still not well understood.

Ideally, an image-guided kidney surgery system would not only account for the changes in kidney position and orientation by performing a rigid alignment, but also for any non-rigid deformation that occurs during surgery. This non-rigid deformation may be caused by external forces applied to the kidney (e.g. by surgical tools, retractors, laproscopic insufflation), by physiological changes, or by other surgical conditions.

One surgical condition in particular that may cause non-rigid kidney deformation is the clamping of the renal artery. Surgeons often clamp the renal artery and vein in order to limit the blood loss during partial nephrectomies. Clamping the renal vessels causes a loss of kidney perfusion such that when the kidney is punctured (e.g. when it is cut with a scalpel), the subsequent drainage of blood could cause a decrease in pressure and deformation of the organ.

However, as the extent and causes of any non-rigid kidney deformation are not well known, the goal of the third section of this work (Chapter 5) was to (a) measure the extent of non-rigid kidney deformation in perfused, ex-vivo kidneys and (b) attempt to correct for non-rigid deformation using splines and/or models. Preliminary data was collected by perfusing ex-vivo kidneys, clamping the renal vessels, making an incision, and then measuring the resulting deformation. The deformation tracked at surface fiducials was interpolated over the kidney

using splines. In addition, an attempt to predict the deformation using linear elastic models was performed.

In summary, the goals of this work were the following:

1. To evaluate an intra-operative registration method using laser scanning methods in open clinical kidney cases (Chapter 2)
2. To extend the intra-operative laser scanning and registration methods to minimally invasive surgery, using a conoscopic laser to obtain kidney surface scans
   a. To develop a novel conoscopic texturing method, in order to enable intra-operative feature-tracking (Chapter 3)
   b. To evaluate the feasibility of using textured conoscopic scanning in-vivo, laparoscopic conditions for intra-operative registration (Chapter 4)
3. To investigate non-rigid kidney deformation in order to evaluate the need for deformation correction in image-guided systems (Chapter 5)

References

[1]   American Cancer Society. 2007. "Cancer Facts and Figures." www.cancer.org.

[2]   Becker, F., Siemer, S., Humke, U., et al. "Elective nephron sparing surgery should become standard treatment for small unilateral renal cell carcinoma: Long-term survival data of 216 patients." Eur Urol. 49(2), 308-13 (2006).

[3]   Lau, W.K., Blute, M.L., Weaver, A.L., Torres, V.E., Zincke, H. "Matched comparison of radical nephrectomy vs nephron-sparing surgery in patients with unilateral renal cell carcinoma and a normal contralateral kidney." Mayo Clin Proc. 75(12), 1236-42 (2000).

[4]   Becker, F., et al., *Elective nephron sparing surgery should become standard treatment for small unilateral renal cell carcinoma: Long-term survival data of 216 patients.* Eur Urol, 2006. **49**(2): p. 308-13.

[5]   Dunn, M.D., et al., *Laparoscopic versus open radical nephrectomy: a 9-year experience.* J Urol, 2000. **164**(4): p. 1153-9.

[6]   Benway, B.M. and S.B. Bhayani, *Robot-assisted partial nephrectomy: evolution and recent advances.* Curr Opin Urol. **20**(2): p. 119-24.

[7]   Scoll, B.J., et al., *Robot-assisted partial nephrectomy: a large single-institutional experience.* Urology. **75**(6): p. 1328-34.

[8]   Hajnal, J.V., & Hill, D. L.G. (2001). *Medical Image Registration*. Boca Raton, FL: CRC Press.

[9]   Besl, P.J., McKay, H. D. (1992). A method for registration of 3-D shapes. IEEE PAMI, 14(2): 239-256.

[10]   Kos, S., et al., *MR-guided endovascular interventions: a comprehensive review on techniques and applications.* European Radiology, 2008. **18**(4): p. 645-657.

[11]   Peters, T. and K. Cleary, eds. *Image-Guided Interventions*. 2008, Springer: New York. 557.

[12]   Ding, S., et al., *Semiautomatic registration of pre- and postbrain tumor resection laser range data: method and validation.* IEEE Trans Biomed Eng, 2009. **56**(3): p. 770-80.

[13]   Dumpuri, P., et al., *Model-updated image-guided liver surgery: preliminary results using surface characterization.* Prog Biophys Mol Biol. **103**(2-3): p. 197-207.

[14]   Clements, L.W., et al., *Robust surface registration using salient anatomical features for image-guided liver surgery: algorithm and validation.* Med Phys, 2008. **35**(6): p. 2528-40.

[15]   Sirat, G.Y., *Conoscopic Holography .1. Basic Principles and Physical Basis.* Journal of the Optical Society of America a-Optics Image Science and Vision, 1992. **9**(1): p. 70-83.

[16]   Sirat, G.Y. and D. Psaltis, *Conoscopic Holograms.* Optics Communications, 1988. **65**(4): p. 243-249.

[17]   Burgner, J., Simpson, A. L., Fitzpatrick, J. M., Lathrop, R. A., Herrell, S. D., Miga, M. I., and Webster, R. J. III, Conoscopic Holography for Intraoperative Digitization: Characterization and Application for Registration. (Submitted to International Journal of Medical Robotics and Computer Assisted Surgery, Dec. 2011.)

[18]   Simpson, A.L., Burgner J., Glisson, C. L., Pheiffer, T.S., Herrell, S.D., Webster, R. J. III, Miga, M. I. A Comparison Study of Contact and Non-Contact Surface Acquisition Methods with Application to Image-Guided Interventions. (Submitted to IEEE Transactions on Biomedical Engineering, Nov. 2011.)

[19]   Simpson, A. L., Burgner, J., Chen, I., Pheiffer, T. S., Sun, K., Thompson, R.J., Webster, R. J. III, Miga, M. I. (2012) Intraoperative Brain Tumor Resection Cavity Characterization with Conoscopic Holography, SPIE Medical Imaging, Feb. 4-9, San Diego, CA.

[20]   Farshad, M., Barbezat, M., Flueler, P., Schmidlin, F., Graber, P., Niederer, P. (1999) Material characterization of the pig kidney in relation with the biomechanical analysis of renal trauma, *J Biomech*. 32(4), 417-425.

[21]   Miller, K. (2000). Constitutive modeling of abdominal organs, *Journal of Biomechanics*. 33:367-373.

CHAPTER 2

INTRAPROCEDURAL REGISTRATION FOR IMAGE-GUIDED KIDNEY SURGERY

Introduction

Mechatronic devices used for medicine, whether they are robots, remote manipulators, laparoscopic assistants or other devices have become more useful as their design allows them to be more "knowledgeable" about their environments and tasks. Perhaps the most successful mechatronic device (at least in sales dollars) has been Intuitive Surgical's daVinci robot. Yet even that device is limited by the guidance system which can only locate objects visible on the surface of structures or on the surface of a cavity created by insufflation. Critical to the future expansion of such device usage is the ability to find an object beneath an opaque surface or at least display the location of that object to the user. By integrating techniques from image-guided surgery with mechatronic devices, the advantages of these devices can be brought to a larger number of applications.

Central to any image-guided surgical procedures is the task of determining the mathematical relationship between image space and physical space. This determination is called a registration, and is generally composed of a single translation vector and a single rotation matrix. The transformation matrix containing the translation and rotation can be obtained by the use of landmarks [1], extrinsic reference objects called fiducials [2], object features such as surfaces [3] or user specified features which possess relevant characteristics [4]. With the ongoing improvement of medical tomograms and the development and improvement of localization devices, either optical or magnetic, the concern in the development of any new image-guided procedure is the ability to obtain a registration and then to identify and deal with any peri-procedural changes such motion or organ deformation which

may degrade or invalidate that registration. In general, registration in abdominal organs has been attempted by either localization of vessel bifurcations [5], pure surface-based registration [6] or by capturing some of the surgeons' understanding of organ shape [7].

Point-based registration has several advantages over other methodologies. Because it is a closed form calculation it is fast and deterministic. By having a surfeit of points for the registration, points can be held out of the registration and used to test the accuracy of the registration by the calculation of a Target Registration Error (TRE) [8]. Surface-based methodologies are iterative in nature, computationally intense and susceptible to converging to local minima. Techniques such as careful selection of the starting pose of the registration and the use of accelerated search methodologies such as K-D trees [9] can mitigate the first two problems. The challenge of quantitatively assessing the accuracy of a surface registration in any given instance remains. In this document we describe our methods for addressing this task.

We have been exploring the task of registration in the kidney for the past several years. A number of ways of obtaining the surfaces and features used for the registration have been developed, and we have analyzed data in phantoms, isolated, perfused pig kidneys, and in human subjects.

Methods

Phantom Experiments

Bringing image guidance to the kidney poses some specific challenges. First, unlike any previous image-guided surgery target, the kidney is covered in perinephric fat, which hinders access to the surface of the kidney and localization of specific anatomic surface targets. The fat also is mechanically coupled to the abdomen and diaphragm, resulting in significant movement with respiration.

Second, the kidney is a smoothly curved structure and surface-based registrations are sensitive to rotational symmetries. The combination of the first and second challenges means that any registration process is going to require exposure of the kidney from its surrounding fat

and the determination of how much and what areas of exposure are required to accomplish an accurate registration.

We have the ability to create anthropomorphic kidney phantoms using a tissue-mimicking silicone (Ecoflex, Smooth-On Inc, Easton, Pennsylvania 18042). Because we created the phantoms (Figure 1) we could place internal targets, and by rigidly attaching the phantom to external frame work we could have external targets as well.

These experiments are described in detail by Benincasa, et al [10]. The internal targets allowed us to estimate application accuracy for image-guided kidney surgery. Because of the greater distance from the center of the organ to the external targets, they are more sensitive to rotational errors than internal targets. Surface registrations are prone to error in rotationally symmetric applications, so by using the external fiducials we maximize our sensitivity to rotational error. Computed tomography (CT) scans of the phantom were taken; the fiducials and outline of the phantom were segmented and localized. A tessellated surface was created from the phantom outlines. Using a tracked laser range scan (LRS) [11] and an optically-tracked probe, the physical surface of the phantom and location of the fiducials were found in the same frame of reference. Iterative Closest Point (ICP) [3] registrations were performed with successively smaller percentages of the surface used and the TREs to the external targets calculated.
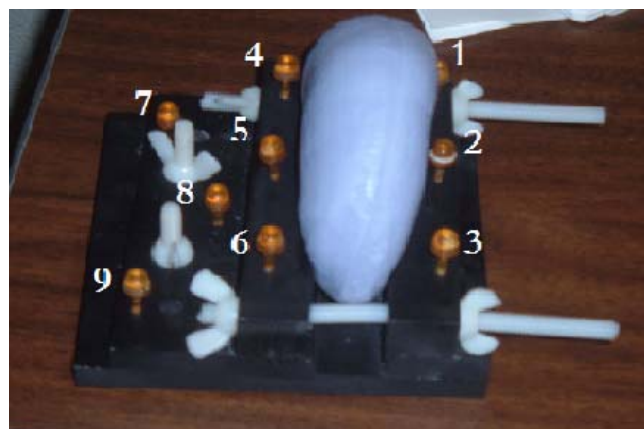
Figure 1. Kidney phantom rigidly attached to a fixture with external fiducials (1-9).

Animal Experiments

While phantoms can be made out of materials which have the same compressibility as a kidney, it is difficult to exactly model the perinephric fat, the loss of turgor in the kidney with the clamping of blood vessels, and the motion and deformation of the kidney due to physiologic events such as breathing or tractions placed on the kidney during the surgery. The use of animal studies represent a midpoint assessment to evaluate our approaches prior to moving to human studies

We have conducted a number of preliminary studies using a porcine animal model. Swine were chosen as their kidneys closely approximate the size and structure of human kidneys. The first experiment assessed the effect of the loss of perfusion associated with standard kidney vessel clamping and a body force similar to the insufflation pressure in a minimally invasive surgery (MIS) application.

Kidneys were obtained from anesthetized or newly euthanized pigs under an IACUC-approved protocol. Heparin was administered intravenously to prevent blood clotting, and the renal artery and vein were tied off to retain turgor before resection. Between 15 and 20 glass beads with 2 mm radii and holes through the center were sutured onto the kidney surface in a roughly even distribution over the entire kidney. CT scans of the kidney (160 or 300 mAs, 90 keV, 0.8 mm slice spacing, Phillips human CT scanner) were taken before and after the kidney drainage. We performed similar experiments incorporating the effect of turgor loss due to an incision.

Human Studies – Open

We have also used two classes of human data for kidney image guidance bystander studies. The first was obtained using an IRB approved methodology for an open kidney partial nephrectomy. In this study we obtained LRS surfaces of a kidney during an open procedure. Since we cannot place extrinsic objects in the kidney prior to surgery, we implemented a different approach for assessment of surface accuracy. Once the kidney was exposed, five dots were placed on the kidney using a surgical marker. We then performed an LRS scan of the kidney. As our LRS obtains a color image which can be texture-mapped onto the 3D surface, the

dots can be localized as virtual fiducials. Figure 2 shows the first registration. The kidney was clamped and cooled as a standard surgical step, and after 10 minutes a second LRS scan was obtained. Finally, the surgery proceeded and the tumor was resected. A final LRS scan was obtained. The ICP algorithm was used to register the LRS scans to the preoperative kidney surface. The stopping criteria for the ICP algorithm was when either (1) the mean distance between points and surface became less than 1x10-7 mm or (2) the number of iterations exceeded 500.

The second human data bystander study involved minimally invasive partial nephrectomy. In an IRB-approved study we have gathered surface data using a daVinci™ (Intuitive Surgical, Sunnyvale, CA) robot in an MIS surgical application.
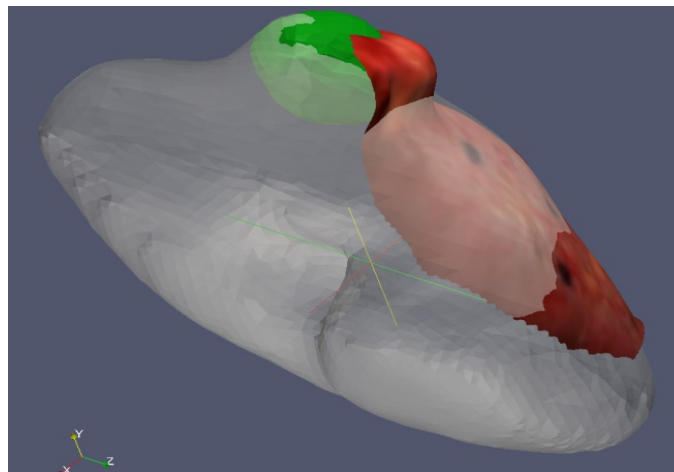
Figure 2. Initial LRS surface (red) registered to CT-derived kidney volume (gray) with tumor (green).

Human Studies – Robotic

In the study, a daVinci™ tool was moved across the surface of a kidney undergoing resection. The surgeon attempted to keep the tip of the tool just resting on the surface. This is both a difficult video processing task given the lack of haptic feedback and a difficult task in controlling the position of the robotic tip. The location of the tool was recorded [12], a sparse surface was created (Figure 3), and this robotically-obtained surface was registered to the pre-operative CT surface using ICP. In Figure 3 the dark blue points were used for the surface registration and the cyan points were held out of the registration. When the transformation

was created, that transformation was applied to the cyan points to see where they would land. In addition, points on or near the vascular insertions into the hilum were marked.
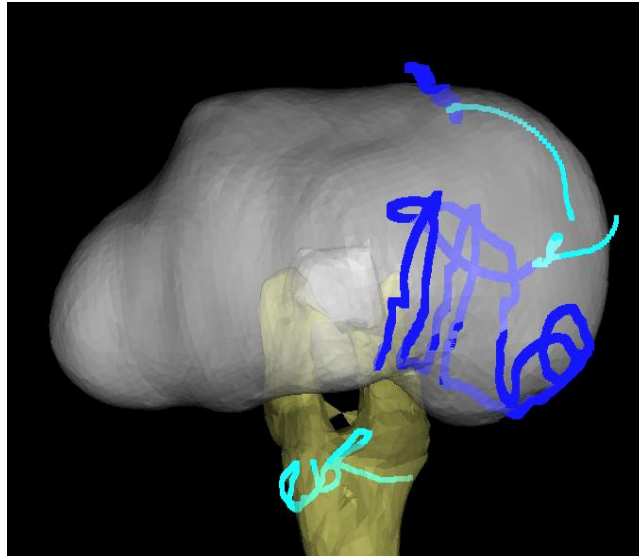
Figure 3. The dark blue lines were used for registration with the CT image. Cyan areas of the kidney and on the hilum were not used to create transformation matrix. Registration was applied to held-out kidney and hilum data.

Results

Phantom Studies

In the phantom trials we repeated registrations 1000 times at each of five different starting poses. The complete observed surface was approximately 84 sq cm. We also varied the percentage of the surface used for the registration. While the post-registration error was, as expected, clearly larger with poor starting poses, if we used more than 17% of the observed surface for registration, the TREs for the final registration proved insensitive to initial pose. We also found that if we used 22% or more of the surface for registration we achieved a minimum TRE of 2.5 mm. This number is based on external fiducials and so overstates the expected error in surgical applications.   Since we know that the accuracy of the surface registrations are really driven by the degree in change in surface curvature, the more highly curved the surface, the more likely registration will be accurate. Therefore it was possible to select areas of the kidney,

13

such as the lateral border, to maximize the registration accuracy for any given surface percentage.

Animal Studies

We performed both ex vivo and in vivo porcine experiments. In the first experiment we perfused an ex vivo kidney to normal perfusion pressures and obtained a CT scan of the turgid kidney. The perfusion sources were clamped, an incision was made in the kidney, and another post-incision CT scan was taken (Figure 5). The glass beads were localized in both scans. As the kidney was fixed, both pre- and post-incision scans were in the same physical space and no registration was necessary. The surface displacement caused by drainage as tracked by the glass beads was calculated, and the distribution can be seen in Figure 6a. The displacement ranged from close to zero to 11 mm with a mean of 6.7 mm and standard deviation of 2.4 mm.

An examination of the displacement field showed that the surface of the kidney moved almost exclusively in the direction of gravity. Figure 6b shows the fiducial errors after applying a simple one-dimensional correction to the surface. It should be noted at this point that the correction was not intended to deal with incisions, therefore the residual error at the opening is to be expected. We are currently developing more sophisticated biomechanical models to correct for this deformation [13].

Table 1. Surface displacement due to clamping and incision in porcine kidneys.

	Displacement due to incision (mm)		
	Mean	Max	Std dev
Pig 1	4.7	9.2	2.2
Pig 2	3.4	2.0	7.4
Pig 3	6.7	11.4	2.4
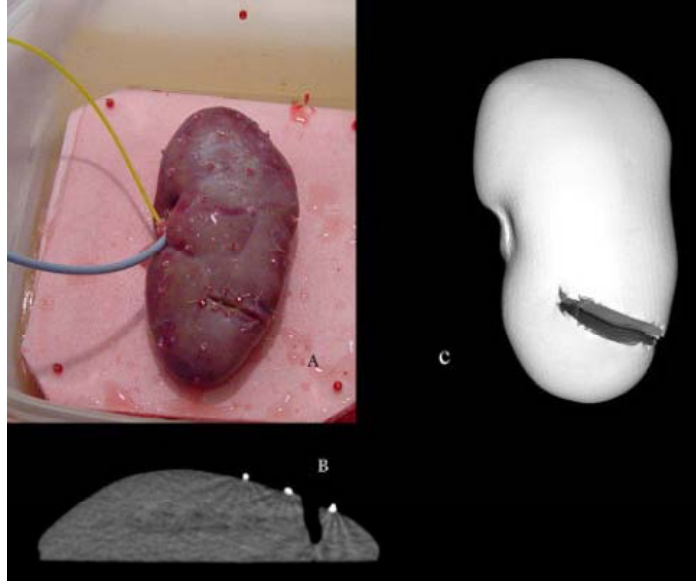
Figure 5. Incised kidney. A) shows the kidney and the fiducial positions (red beads). B) shows a CT scan to show the depth of the incision while c) is a rendering of the full CT.
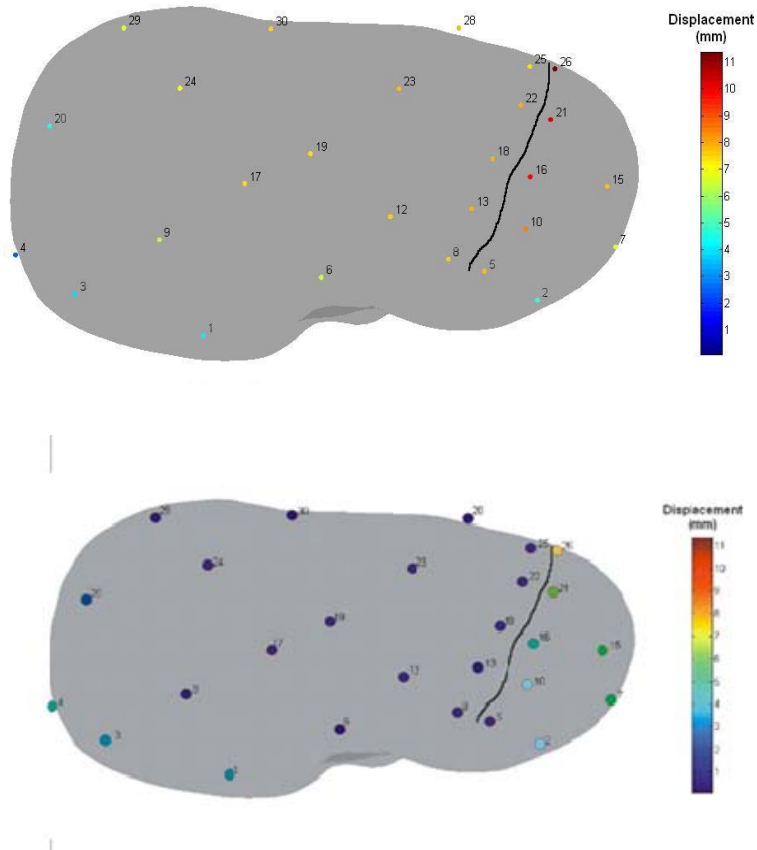
Figure 6 (a) (top) shows the surface displacement at each numbered fiducial after an incision into a kidney (mean displacement: 6.7 mm). (b) (bottom) shows the error after a simple one-dimensional correction.

15

Human Studies – Open

       In a human application, it is difficult to establish a true target that is easily localizable in both the image and physical spaces. Anatomic structures such as the insertion points of major vessels into the kidney at the hilum can serve as approximate targets but the Target Localization Error for such points can confound determination of registration error. As a step to address that we have developed the ideas of "virtual fiducials." Because our phantom and animals studies showed that a complete surface scan could be accurately mapped to a tessellated surface extracted from a tomographic image set, we accepted our initial registration in open procedures as the gold standard. Once we opened the patient we placed five dots on the surface of the kidney as fiducials.   When the LRS maps the surface of the kidney, it also obtains a color image which can be texture mapped onto the 3D surface. This lets us assign three dimensional values to the dots, and via the "gold standard" registration, assign those dots to image-space coordinates. A relative TRE can then be calculated for all subsequent registrations using the virtual fiducial locations. Figure 2 shows the first "gold standard" registration of the LRS scan using ICP.

       Subsequently, the vascular supply to the kidney was clamped and the kidney iced as the standard surgical procedure. After 10 minutes, a second LRS scan was obtained. This post-clamp LRS surface was registered to the preoperative CT surface using ICP. The virtual fiducials were localized, and the mean relative TRE for this process was 0.95 mm with a max of 1.33 mm and standard deviation of 1.33mm. Figure 7 shows the registration after clamping and cooling.
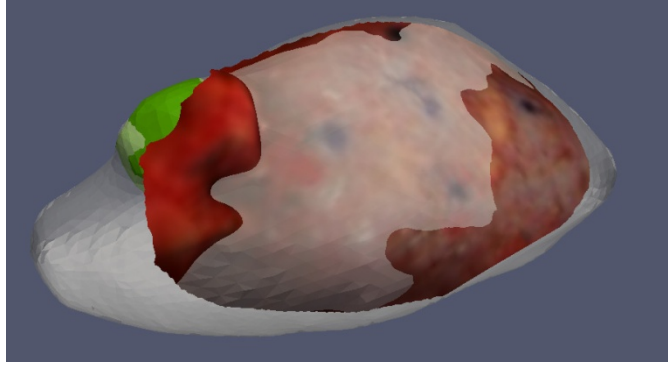
Figure 7. LRS surface (red) registered to preoperative image surface (gray) after clamping of the renal vessels and icing. Tumor is shown in green.
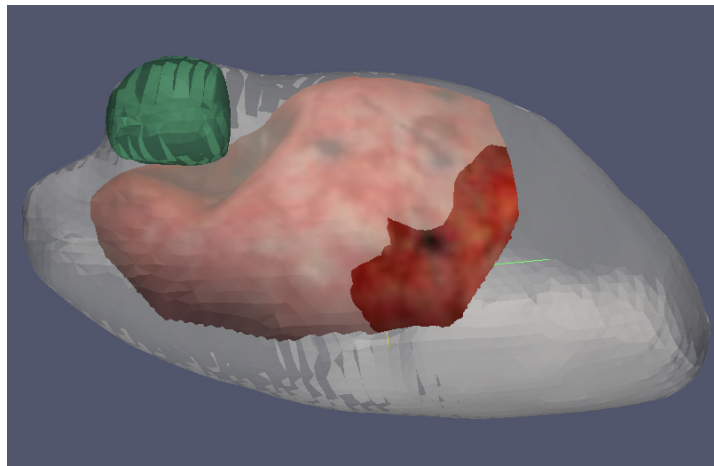
Figure 8. Post resection LRS registered to the preoperatively obtained surface. Notice that the LRS surface appears to exist beneath the preoperative surface.

Table 2. Human open nephrectomy registration error. The post-clamp and post-resection LRS surfaces were registered using point-based virtual fiducial method.

	Closest distance (mm)			Relative TRE (mm)		
	Mean	Std	Max	Mean	Std	Max
Pre-clamp (ICP)	0.9	0.8	5.3	--	--	--
Post-clamp (virtual fiducial)	1.0	0.9	5.6	0.95	0.39	1.3
Post-resection (virtual fiducial)	1.0	0.7	3.2	7.3	2.0	9.5

Finally, the surgery proceeded and the tumor was resected. A post-resection LRS scan was obtained. After the resection, the surface had a significant resection crater which impeded

the ICP surface registration (mean, standard deviation, and maximum relative TRE of 7.33 mm, 1.99, and 9.53mm, respectively). This can be seen in the registration image in Figure 8 where the registered LRS surface seems to "dive" under the surface of the CT-derived surface.

However, we know that an accurate registration could still be performed even after the resection due to use of the virtual fiducials in a point-based registration. Using the virtual fiducials to register the post-clamp surface via a point-based method resulted in mean closest point distance of 1.0 mm (standard deviation 0.9 mm, max 5.6 mm). Similarly, the post-resection point-based registration resulted in a mean closest point distance of 0.97 mm (standard deviation 0.7mm, max 3.2 mm). Registrations using the virtual fiducials have the potential of not being as impeded by changes in kidney shape caused by resections. For instance, spline-based methods are being explored to more accurately register post-resection scans. Further studies are planned where we will place more virtual fiducials   away from the resection cavity in order to track the deformations.

Human Studies – Robotic

The use of the robot for image-guided surgery presents two additional difficulties to our earlier work. Both arise from the fact that the surfaces cannot be obtained at this time using a Laser Range Scanner. Therefore we have to use points obtained by dragging a daVinci™ instrument over the unveiled surface of the kidney and recording its location. This means that the surface will lack the dense point cloud provided by the LRS, and we will not get as complete a surface as we had for the open surgeries in both the animal and human models. The second issue is that we are tracking the tip of the instrument, presuming that the tip is always co-incident with the organ surface. In fact, the tip can float off the surface and occasionally press into the surface, reducing the accuracy of the surface registration. This can be seen in figure 3, where the dark blue line seems to curl off the kidney at the top of the picture. However, the results of this registration are qualitatively very good. The mean closest point distance was found to be 1.4 mm with standard deviation of 1.1mm. We held out the points represented in cyan and only used the dark blue ones for the registration. We then used the transformation

obtained from the dark blue points and applied it to the cyan points which include the vascular locations beyond the hilum. Those points qualitatively aligned with the intended target.

Table 3. Human robotic study; results of ICP registration.

	Closest distance (mm)	
	Mean	Std
Patient 1	1.4	1.1
Patient 2	1.2	0.9

Discussion

The surgical driving force behind this development is the growing realization of the importance of sparing healthy nephrons from damage in surgery while simultaneously avoiding damage to a tumor capsule and obtaining a clear resection margin. However, there are several technical challenges associated with these procedures including adequate intraoperative identification of the margins of the diseased tissue, identification and control of the vascular supply, and avoidance of ischemic injury to the normal kidney tissue [1]. Currently, surgeons remove the diseased tissue using visualization, either direct or laparoscopic. The appearance of diseased and normal tissue may not be significantly different which can prolong the procedure and decreases the likelihood of a clear margin without significant excess healthy tissue damage. Surgeons are often resecting a target that they can barely see unless they significantly disturb healthy tissue. The less the surgeons are required to disturb the kidney and its surrounding tissue during the procedure, the lower the risk for subsequent kidney morbidity. Thus, there remains a need to improve intraoperative visualization of the kidney in order to improve surgical outcome; for example, this may include a display of the present position of surgical instruments using the three dimensional data of the preoperative tomograms. Employing image-guided surgery techniques, which are now a standard in neurosurgery and emerging in other abdominal surgeries, could provide this visualization during the procedure.

The largest source of surgical morbidity for either resection or ablation is vascular injury [2]. Therefore, both the success of the resection and the minimization of morbidity would be augmented by active display of surgical tool position relative to the location of the preoperatively determined surgical margin and the surrounding vasculature. As a result more partial nephrectomies could be performed for renal masses currently treated with radical nephrectomy. Vascular damage could be minimized and greater renal function preserved, resulting in improved patient outcomes.

To bring the advantages of intraprocedural tracking on high resolution preoperative imaging to kidney applications, a methodology for registering the spaces must be developed. That methodology must reliably create accurate registrations providing the surgeon with some feedback of expected maximum error. Other laboratories are working on methods of using tomographic calibrations, that is, understanding the relationship between a surgical target seen in a scan and its location in the scanner [12,13].

The entire error of the clinical registration system using virtual fiducials is difficult to determine; however, the mean closest distance of the ICP and point-based registrations are reported in the results. In addition, the Polaris tracking error as reported by the Northern Digital specifications is 0.25mm RMS (95% confidence interval of 0.5mm).; the LRS error is 1.4±0.8 mm [11]; and the DaVinci FLE is 1.05mm [12].

As this unique type of clinical data has not been published in the literature, we feel the preliminary results of this study are exciting and important to report in a research journal. We have also supplemented and completed the studies with more controlled scenarios: animal and phantom studies.

With the trend towards procedures of decreasing invasiveness, there will be smaller and smaller exposures during surgery. Tools, both physical and mathematical, must be developed so that image-guided surgery and minimally invasive surgery are compatible and not competing.

Work is ongoing to develop non-contact tools and to refine surface identification and localization so that less of the surface has to be exposed for registration. In addition, we are developing mathematical models with our colleagues which can function in surgery-appropriate

20

time periods to account for intraoperative kidney deformation due to resection. All of these developments will provide greater surgical confidence for precise lesion resection.

Acknowledgments

References

[1]   Neelin P, Crossman J, Hawkes DJ, Ma Y, Evans AC, Validation of an MRI/PET landmark registration method using 3D simulated PET images and point simulations. Comput Med Imaging Graph 1993 Jul-Oct;17(4-5):351-6

[2]   Maurer CR Jr., Fitzpatrick JM, Wang MY, Galloway RL, Jr., Maciunas RJ, and Allen GS. Registration of head volume images using implantable fiducial markers. IEEE Transactions on Medical Imaging, 16:447-462, 1997.

[3]   Besl, PJ, McKay, HD, "A method for registration of 3-D shapes". IEEE PAMI Feb 1992 Vol:14, No.2 pp 239-256

[4]   Maurer CR Jr, Maciunas RJ, Fitzpatrick JM."Registration of head CT images to physical space using a weighted combination of points and surfaces." IEEE Trans Med Imaging. 1998 Oct;17(5):753-61.

[5]   Lange T, Papenberg N, Heldmann S, Modersitzki J, Fischer B,Lamecker H and Schlag PM, "3D ultrasound-CT registration of the liver using combined landmark-intensity information". IJCARS , Volume 4, Number 1 / January, 2009 pp 79-88

[6]   Herring JL, Dawant BM, Muratore D, Maurer CR, Galloway RL, and Fitzpatrick JM, Surface-based registration of CT images to physical space for image-guided surgery of the spine, IEEE Transactions on Medical Imaging 17, 5, pp. 743-752, 1998

[7]   Clements LW, Chapman WC, Dawant BM, Galloway RL, and Miga MI, "Robust surface registration using salient anatomical features for image-guided liver surgery: Algorithm and validation," Medical Physics, vol. 35, pp. 2528-2540, 2008.

[8]   West JB, Fitzpatrick JM, Toms SA, Maurer CR Jr, Maciunas RJ. "Fiducial point placement and the accuracy of point-based, rigid body registration". Neurosurgery 2001 Apr;48(4):810-6; discussion 816-7.

[9]   Sinha TK, Cash DM, Weil RJ, Galloway RL, Miga MI, Cortical surface registration using texture mapped point clouds and mutual information, Lecture Notes in Computer Science Lecture Notes in Computer Science: Medical Image Computing and Computer-Assisted Intervention – MICCAI 2002, Springer Verlag, New York, Vol. 2489, Part 2, pp. 533-540, 2002.

[10]   Benincasa AB, Clements LW, Herrell SD, Galloway RL. Feasibility Study for Image-Guided Kidney Surgery: Assessment of Required Intraoperative Surface for Accurate Physical to Image Space Registration. Medical Physics Sep;35(9):4251-61 2008.

[11]   Cash DM, Sinha TK, Chapman WC, Terawaki H, Dawant BM, Galloway RL, Miga MI, Incorporation of a laser range scanner into image-guided liver surgery: Surface acquisition, registration, and tracking, Medical Physics, vol. 30(7), 1671-1682 2003

[12]   Kwartowitz DM, Herrell, SD, Galloway RL "Towards Image-guided Robotic Surgery: Determining Robot Accuracy". International Journal of Computer Assisted Radiology and Surgery Volume 1, Number 3 / November, 2006 pp 157-165.

[13]   Ong, R. E., Glisson, C. L., Herrell, S. D., et al., "A deformation model for non-rigid registration of the kidney," Proceedings of SPIE Vol. 7261, 72613A (2009).

[14]   Teber D, Guven S, Simpfendörfer T, Baumhauer M, Güven EO, Yencilek F, Gözen AS, Rassweiler J. Augmented reality : A New Tool To Improve Surgical Accuracy During Laparoscope Partial Nephrectomy? Preliminary InVitro and InVivo Results Eur Urol. 2009 Aug;56(2):332-8. Epub 2009 May 19

[15]   Patriciu A, Solomon S, Kavoussi L, Stoianovici D. Robotic Kidney and   Spine Percutaneous Procedures Using a New Laser-Based CT Registration Method. Lecture Notes in Computer Science Volume 2208/2010 Pages 249-257, 2001

CHAPTER 3

A NOVEL METHOD FOR TEXTURE-MAPPING CONOSCOPIC SURFACES

Rowena E. Ong, Courtenay L. Glisson, Jessica Burgner, Mark Sawyer, Amber Simpson, Ray Lathrop, Andrei Danilchenko, S. Duke Herrell, Robert Webster, Robert L. Galloway

INTRODUCTION

A growing number of surgeons are using minimally invasive approaches for the surgical treatment of kidney cancer. Because of the smaller incisions made and the healthy tissue saved, these surgeries have been shown to result in faster recovery times, better post-operative renal function, and reduced scarring compared to open procedures [1, 2]. However, the challenges in terms of surgical dexterity, visualization and orientation in an unevenly-illuminated cavity, and the manipulation of multiple tools in a small space can make minimally invasive surgery difficult. Laparoscopy's widespread usage has been facilitated by robotics, which allow for finer control of tools through small ports [3, 4]. Incorporating image guidance into MIS could provide further benefits by allowing surgeons to more easily orient themselves, visualize tumor margins, and avoid critical healthy structures such as vessels.

Previous work in image guidance for soft tissue has shown promising results, and image guidance is currently commercially available for applications such as intracranial, ENT, orthopedic, and liver procedures (Medtronic Navigation, Louisville, CO; BrainLab, Feldkirchen, Germany; Pathfinder Therapeutics, Nashville, TN). However, one of the central challenges for developing soft tissue guidance is the deformation the organ may undergo during the surgery. To track this deformation, different methods such as ultrasound, intraoperative CT, bi-planar fluoroscopy, laparoscopic camera, electromagnetic tracking, and intraoperative MR have been explored. However, each has its limitations: ultrasound has limited imaging capabilities, signal to noise, and measurement challenges due to velocity changes through tissue; laparoscopic camera and fluoroscopy provide only 2D images which can be difficult to use for navigation;

intraoperative CT and fluoroscopy involve radiation exposure to patient and surgeon; intraoperative MR requires an MR-compatible operating suite and has patient access challenges [5]; and electromagnetic tracking can be limited by a small tracking volume [6].

To overcome these limitations, a laser range scanner (LRS) has been used for collecting intraoperative data useful for navigation. It has successfully been used in liver and brain registrations [7-9].

Although the LRS is a promising method for intraoperative data collection, it is too large to be used through a laparoscopic port. To address this issue, we have been exploring conoscopic holography for intraoperative data collection in minimally invasive surgeries. Conoscopic holography is a method for measuring the distance to an object at a single point using a reflected laser beam. In this method, the reflected light is passed through a polarizer and crystal, and the resulting phase changes and interference pattern can be used to calculate the distance to the object [10, 11]. Unlike the LRS, which uses a stereoscopic method to calculate distance necessitating a large intraocular distance, the conoscopic laser can be made small enough to fit through a trocar port (Figure 1).   When optically tracked, the conoscopic can be swept across an organ surface to obtain a 3D point cloud. A study of the geometric accuracy of the conoscopic surfaces can be found in [13], and registration accuracy studies have also been performed [14].
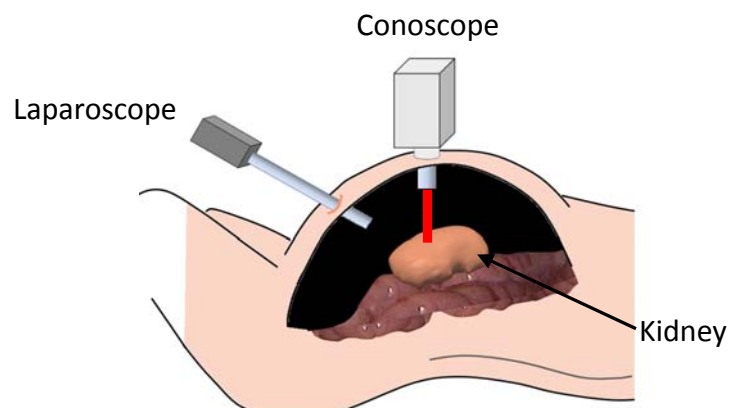
Figure 1. Diagram showing insufflated abdomen with conoscopic laser and laparoscope used through trocar port.

Although these results are promising, the conoscope only gives a point cloud for use in surface-based registration. While this is useful for registration in some applications, the kidney's smooth, uniform shape and lack of geometric features may limit the accuracy of a pure surface-based registration such as Iterative Closest Point (ICP). To remedy this problem, this paper presents a novel method of texture-mapping conoscopic surfaces using a laparoscopic camera. The purpose of obtaining the texture map is to track texture features, natural or artificial, to aid in the registration of the kidney during gross movement or deformation in surgery.

In this paper, we present a novel method of texture-mapping a conoscopic surface using a laparoscopic camera. The calibration and accuracy of the method are investigated using ex-vivo porcine and human cadaver kidneys. Finally, the accuracy of a feature-tracking registration scheme using the textured conoscopic surface is reported. While this paper focuses on kidney applications, this method could be applied to other abdominal organs such as the liver.

METHODS

Conoscopic Hardware

A commercially available conoscope (Probe Head Mk3, OPTIMET, North Andover, MA) was used. To track its 3D location, a Polaris (Northern Digital, Ontario, Canada) passive rigid body was attached to the body of the conoscope (Figure). A sterilizable, airtight attachment was constructed to facilitate its use through a laparoscopic trocar port. The conoscope data rate can be set as high as 1000 Hz, but for these experiments, we used a frequency of 400 Hz.

Figure 2. Conoscope with Polaris rigid body attached.

Texture Mapping Algorithm

Overview

In this method, an optically tracked conoscope is swept across a surface to obtain a 3D point cloud. This point cloud is then texture-mapped using the video obtained from a laparoscopic camera (Figure 3). To texture-map the point cloud, we use the fact that that each 3D point has a corresponding video frame in which the red laser dot is seen. From the segmented red dot, the texture coordinates of the point can be determined, and a color can be assigned from either a reference image or a previous frame. In our implementation, we assume the laparoscopic camera is fixed during the data acquisition, and we assign the texture from a reference image taken before the conoscope acquisition. However, future improvements could allow the laparoscopic camera to be tracked, eliminating the need for a fixed camera during the acquisition.
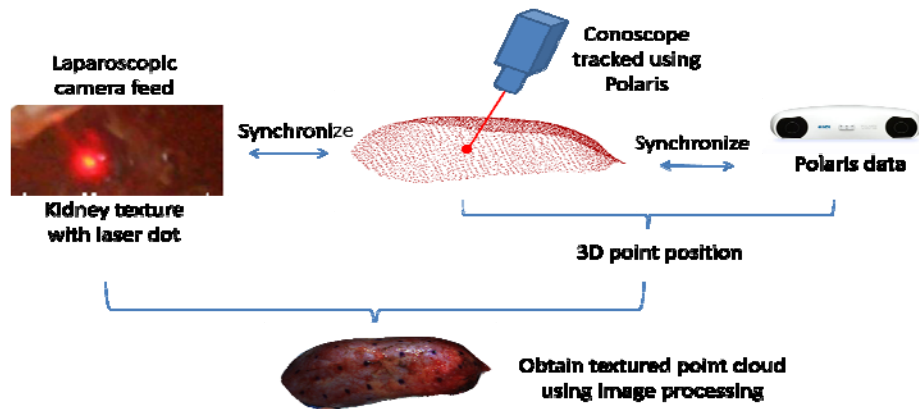
Figure 3. Diagram illustrating texture-mapping algorithm. An optically tracked conoscope is swept across a surface to obtain a 3D point cloud. The corresponding video frames, from which the red laser dot can be localized, are used to assign a color to each point.

Infrared Tracking

In order to obtain a 3D point cloud, the conoscope was tracked using the Polaris Spectra passive infrared tracking system. The conoscope itself yields a distance measurement at a single point, representing how far an object is from conoscope's reference plane. In order to transform that distance measurement into a 3D coordinate space, the corresponding location of the attached Polaris rigid body was obtained. To obtain the transformation from the Polaris rigid body center to the conoscope origin, a calibration was performed using a pivot technique. The details and accuracy of this calibration can be found in [13].

Laparoscopic Video Collection

To collect the laparoscopic video, an Elgato Video Capture frame grabber that ports S-video to USB was used. A program was written to capture the video stream using DirectShow libraries in Windows 7. The laparoscope control units used were either a Karl Storz Telecam ntsc or Tricam SL ntsc, and a Karl Storz Xenon Light Source 615 or 175 was used. The laparoscope was run at a frequency of 30 frames/sec.

Synchronization

One of the most important steps in this algorithm is the synchronization of the conoscope, Polaris, and laparoscopic video streams. The conoscope and Polaris data streams

must be synchronized to ensure an accurate 3D point location, and the video stream must be synchronized to ensure that the color assigned to each point is accurate.

A custom C++ program was written to obtain the conoscopic, Polaris, and video data streams on separate threads. The conoscopic and Polaris data were time-stamped in milliseconds using the standard Windows 7 libraries, which has a time resolution of 1 ms, but typically an accuracy of between 10-16 ms [15]. (In comparison, the Polaris at 60Hz has a sample spacing of about 17 ms, and the conoscope at 400 Hz has a sample spacing of about 2.5 ms.) For the video stream, a time-stamp was obtained at the start of the stream, and the relative timing of the frames was saved as a part of the video format. Each data stream was post-processed to match the frames in each data stream by timestamp.

The frequency of the data streams were as follows: Polaris at 60Hz, conoscope between 400-1000Hz, and video at 30 Hz.

Image Processing

In order to assign each 3D surface point a color, the red laser dot in the corresponding video frame was localized using the difference image between frames. A simple red channel threshold was used to segment the dot, and the centroid was calculated. From this location, the texture coordinates of the point were determined, and a color was assigned from a reference image taken before conoscopic data acquisition. After the texture coordinates are found for the conoscopic point cloud, a radial basis function and meshing algorithm are used to create a smooth, textured triangular surface mesh. Currently a MATLAB and Python script are used in this process.

This method assumes a fixed laparoscopic camera and that the object of interest is not moving during data acquisition. If the laparoscope were tracked, it could freely move; however, for these experiments we elected to fix the laparoscope position.

1. Synchronization Studies

Because the synchronization of the conoscopic, Polaris, and video data streams is so important, we performed a series of tests to quantify the synchronization accuracy. There are several sources of possible synchronization error: (1) Determination of start time of video stream, (2) relative timing of each frame of the video stream, (3) Polaris timing, (4) conoscope timing. These studies are important to determine if there is an offset or drift that we can correct. Once these are corrected, the final synchronization accuracy will place a limit on the accuracy of the texture map as well as the conoscope scanning speed. In addition, characterizing the synchronization error will also help us determine what frame rates we need in the future if a certain scan speed or accuracy is desired.

a. Synchronization test using external blocking event

In the first test, we used an external blocking event to verify the synchronization of the conoscope, Polaris, and video data streams. An object was dropped in front of an aligned Polaris target, conoscope laser, and laparoscopic camera such that it would block the data streams simultaneously. The times of the blocking event were found in each data stream and compared to find the error and any offset. As the conoscope had the highest frequency (400-700 Hz), it was used as the reference and the Polaris and video streams were synchronized to it.

b. Accuracy of relative timing of video stream

In the second test, we wanted to verify the relative timing accuracy of the video stream, in particular to determine if there was a drift or bias in the timing over time. Because only the starting time of the video stream is recorded, it was important to verify the relative accuracy of the timestamps in the saved video format. To do this, we aimed the laparoscopic camera at an external millisecond clock displayed on the screen of a separate laptop. For 3 trials and at 7 different sampling times ranging between 5-180 seconds into the video stream, the difference between the external timer and the internal video timing was determined for a total of 21 samples.

2. Accuracy Studies

As the geometric accuracy of the conoscopic surface has been characterized elsewhere [13], in this paper we will focus on characterizing the accuracy of the texture map.

a. Calibration image

Because the conoscopic surface is made up of single points collected as the conoscope is swept across a surface, the accuracy of the texture mapped surface may be dependent on the density of scan lines or the scan speed. To determine the effect of these factors on the texture accuracy, we used a robot (Mitsubishi RV-3S industrial robot) to move the conoscope at different speeds and different line densities over a colored checkerboard image of known dimensions. For more information on the robot kinematics and setup, please see [12].

To verify the accuracy of a textured surface, the error between known geometry of the checkerboard was compared to that obtained from the textured surface. Specifically, the error was defined as the distance between the square corners localized from the texture and their known locations. The calibration image used was a 5x3 checkerboard colored with red, green, and blue squares printed on flat, white paper. Each square had a width of 13.9 mm.

To access the effect of scan line density on the accuracy of the textured surface, we used the robot to obtain 5 datasets at 10, 5, and 2mm scan line spacings, for a total of 15 data acquisitions. The Polaris, conoscope, and laparoscopic video streams were synchronized, and the conoscopic surface was constructed and textured using the image processing methods described above. The checkerboard corners were localized from the textured surface manually, and the distance from the known locations was calculated.
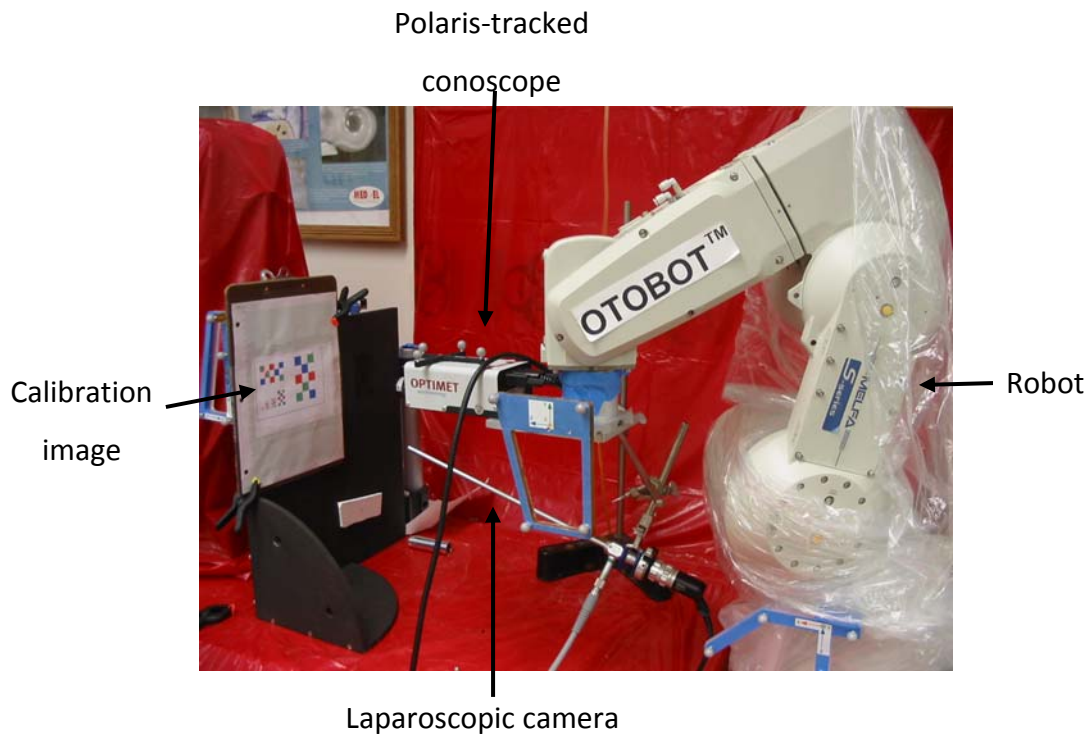
Figure 4. Setup for the image calibration study. The robot aimed the tracked conoscope across the calibration image, and multiple trials were taken using different scan line densities. The video obtained from the laparoscopic camera was used to texture map the conoscopic surface.

b. Ex-vivo porcine kidneys

Because the conoscopic laser may interact with tissue differently than with other materials, it is important to validate our conoscopic texturing method using a more realistic material and geometry. To this end, ex-vivo porcine kidneys (frozen at about -10 C immediately after resection and thawed before use) were scanned with the conoscope and texture-mapped using the presented method. Flat, circular green surface fiducials (diameter 7.2 mm) were marked with an "x" at their centers and used to calculate the texture accuracy. Two methods of validation were used in these studies: (1) comparison of the texture-localized fiducials to a gold standard localized using a probe and (2) comparison to an LRS texture.

i. Validation using probe-localized points

In these studies, 4 ex-vivo porcine kidneys were covered with between 5 and 11 surface fiducials for validation. The fiducial centers were localized using either a Polaris probe or

conoscope as a gold standard, and the error between the texture-localized and gold standard positions was calculated. The error was determined by calculating the target registration error (TRE) of a point-based registration between the texture-localized and gold standard probe-localized fiducials. To do this, one fiducial was designated the target, while the remaining were used in the point-based registration. The procedure was repeated, each time changing the fiducial chosen as the target, so that the leave-one-out TRE could be calculated at each fiducial. The leave-one-out TRE was then averaged over all the trials. The fiducial registration error (FRE) was also calculated.
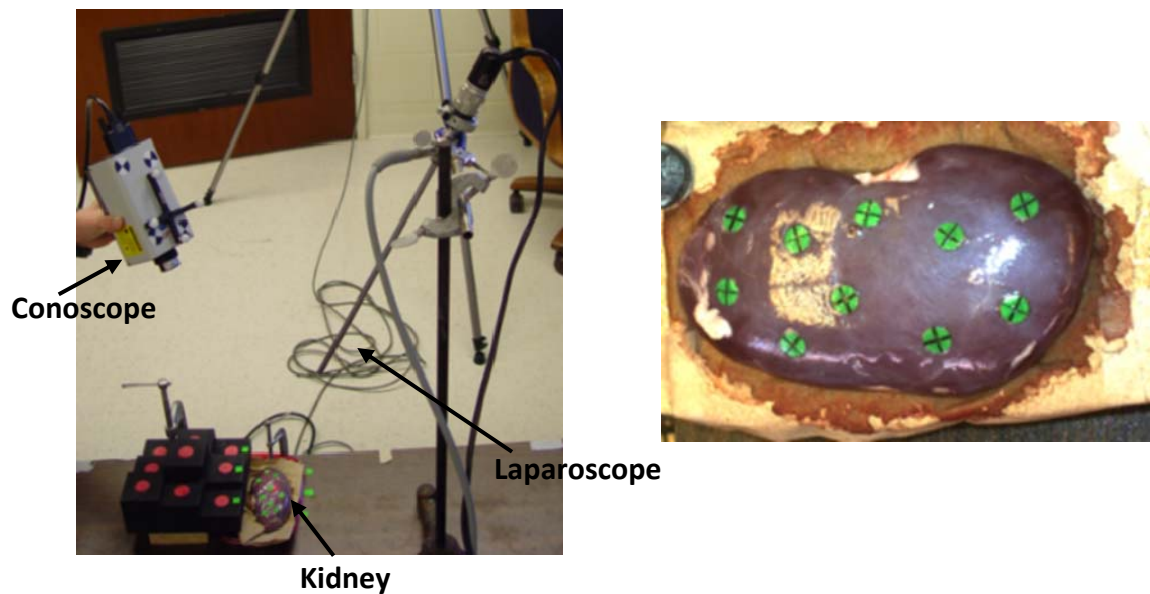
Figure 5. Setup for ex-vivo porcine kidney scans (right) and close-up of porcine kidney covered with circular green surface fiducials (left).

ii. Comparison to LRS

To compare the conoscopic surface to that obtained from a gold standard LRS (Pathfinder Therapeutics, Inc., Nashville, TN), a porcine kidney was covered with 10 fiducials and scanned with a conoscope 5 times, and the reconstructed textured surfaces were compared to an LRS scan. The fiducial centers were localized from both the conoscopic texture and the LRS texture, and a point-based registration was used to align the two coordinate

spaces. To measure the difference between the two surfaces, the FRE and leave-one-out TRE as described in the section above were calculated.

c. Ex-vivo human kidneys

The accuracy of the conoscopic texture mapping was tested using an ex-vivo kidney from a partially fixed human cadaver. To facilitate validation, six fiducials consisting of surgical tape marked with an "x" were attached to the kidney surface, and six conoscopic scans were obtained. The centers of the marks were localized using a Polaris probe, and the error between texture-localized and Polaris-localized points was calculated. The leave-one-out TRE and FRE were calculated.

d. Scanning and post-processing times

The conoscope scanning and post-processing times were recorded for the 10 ex-vivo and 4 human cadaver trials. The post-processing times were subdivided into the running times for the MATLAB and Python scripts. The scripts were run on a Lenovo laptop with an Intel Core i7 processor, 4 GB of RAM, and Windows 7 64-bit operating system installed.
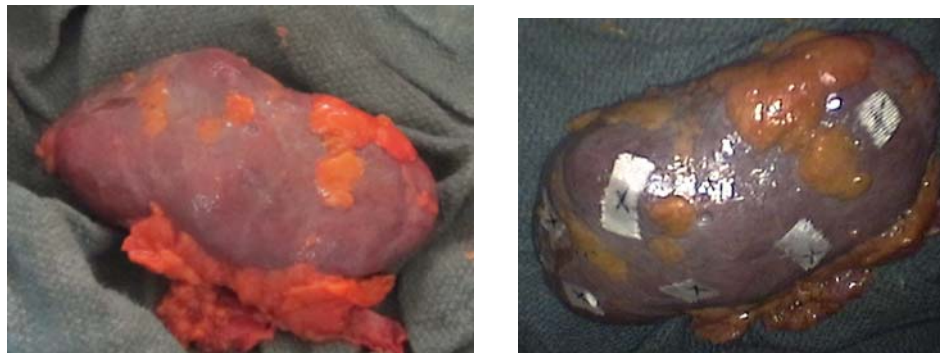
Figure 6. Ex-vivo kidneys from a partially fixed human cadaver to be scanned by the conoscope (left); the same kidney covered with fiducial stickers (right). The peach-colored areas represent the peri-renal fat that had not been completely removed from the kidney.

RESULTS

1. Synchronization Studies

a. Synchronization studies with external blocking event

The synchronization studies indicated a delay in between the Polaris and conoscope

data streams, as shown in Table. The positive sign of the errors indicate the synchronization

event happened earlier in the conoscope data stream than in the Polaris stream, and therefore

it appears that the Polaris stream is lagging behind the conoscope. As the frame rate of the

Polaris was 60 Hz, the mean delay was equivalent to approximately 1.8 Polaris frames.

The video frames also appeared to lag behind the conoscope data, but only by an

average of half a frame (Table 1). Because of the relatively slow video frame rate (30 fps), and

the difficulty in isolating the exact time of the synchronization event in the video frames, the

delay of half a frame may be within the error of the measurements.

Table 1. Difference in the recorded times of a simultaneous external synchronization event between conoscope, Polaris, and video data streams. Positive numbers indicate a lag in the Polaris or video data streams compared to the conoscope stream.

Trial	Conoscope-Polaris Sync Error (ms)	Conoscope-Video Sync Error (frames)
1	17	0
2	47	1
3	40	0.5
4	51	1
5	15	1
6	26	0.5
7	15	1
8	32	0
9	29	0.5
10	20	0
Mean	29.2	0.55
Std.	13.1	0.43

b. Accuracy of the relative timing of the video stream

There was no significant bias in the relative timing of the video, as the mean difference between the external and internal timing was less than a millisecond (-0.4 ms +/- 5.4 ms) over all the samples. There was also no bias or increase in error as the video progressed, as tested up to 180 sec. The standard deviation was about 5 ms, which is within the error of the Windows C++ library used to obtain the times.

2. Accuracy Studies

a. Calibration image

The effects of scan line density on texture map accuracy are shown below (Table 2) for line spacings of 10, 5, and 2 mm. The mean errors in all cases were sub-millimetric (below 0.7mm), and the maximum error did not exceed 2mm. While the mean errors are slightly lower for denser line spacings, an ANOVA test showed that these differences were not significant at the 0.05 confidence level. Some representative textured surfaces are shown in Figure 8. The quality of the texture maps generated from the denser scan lines appears to be slightly better than those generated from the more sparse lines.

Table 2. Effect of scan line density on texture map accuracy, assessed using a checkerboard phantom. The error between checkerboard corners localized from the textured surface and the known locations is shown below, for scan line spacings of 10, 5, and 2 mm. The speed of the robot data acquisition was 40 mm/s.

Scan line spacing	Trial	Error (mm)			
		Mean	Std	Max	Min
10 mm	1	0.73	0.43	1.73	0.19
	2	0.65	0.30	1.24	0.06
	3	0.61	0.39	1.89	0.13
	4	0.68	0.31	1.63	0.30
	5	0.61	0.37	1.74	0.09
	All	0.66			
5 mm	1	0.65	0.37	1.67	0.16
	2	0.57	0.35	1.38	0.10
	3	0.62	0.40	1.59	0.13
	4	0.64	0.33	1.68	0.06
	5	0.63	0.31	1.74	0.12
	All	0.62			
2 mm	1	0.61	0.32	1.47	0.11
	2	0.61	0.35	1.43	0.11
	3	0.61	0.38	1.54	0.08
	4	0.55	0.32	1.46	0.09
	5	0.56	0.36	1.60	0.08
	All	0.59			
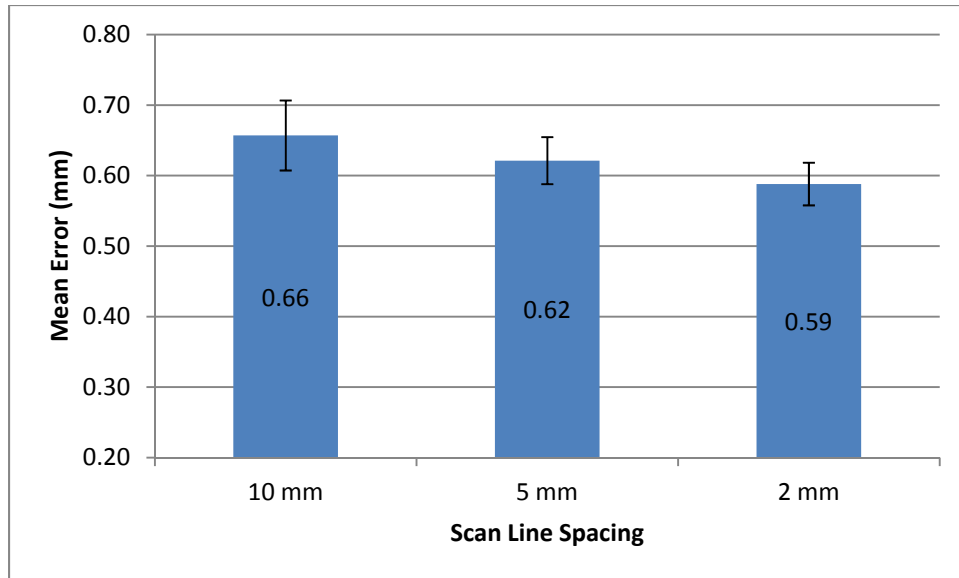
Figure 7. Bar graph showing the effect of scan line density on texture map accuracy, assessed using a checkerboard phantom. The bars show the mean error between texture-localized and known checkerboard corners, for 5 trials taken at scan line spacings of 10, 5, and 2 mm each. The speed of the robot data acquisition was 40 mm/s for all trials. The difference between the groups is not significant at the 0.05 confidence level.
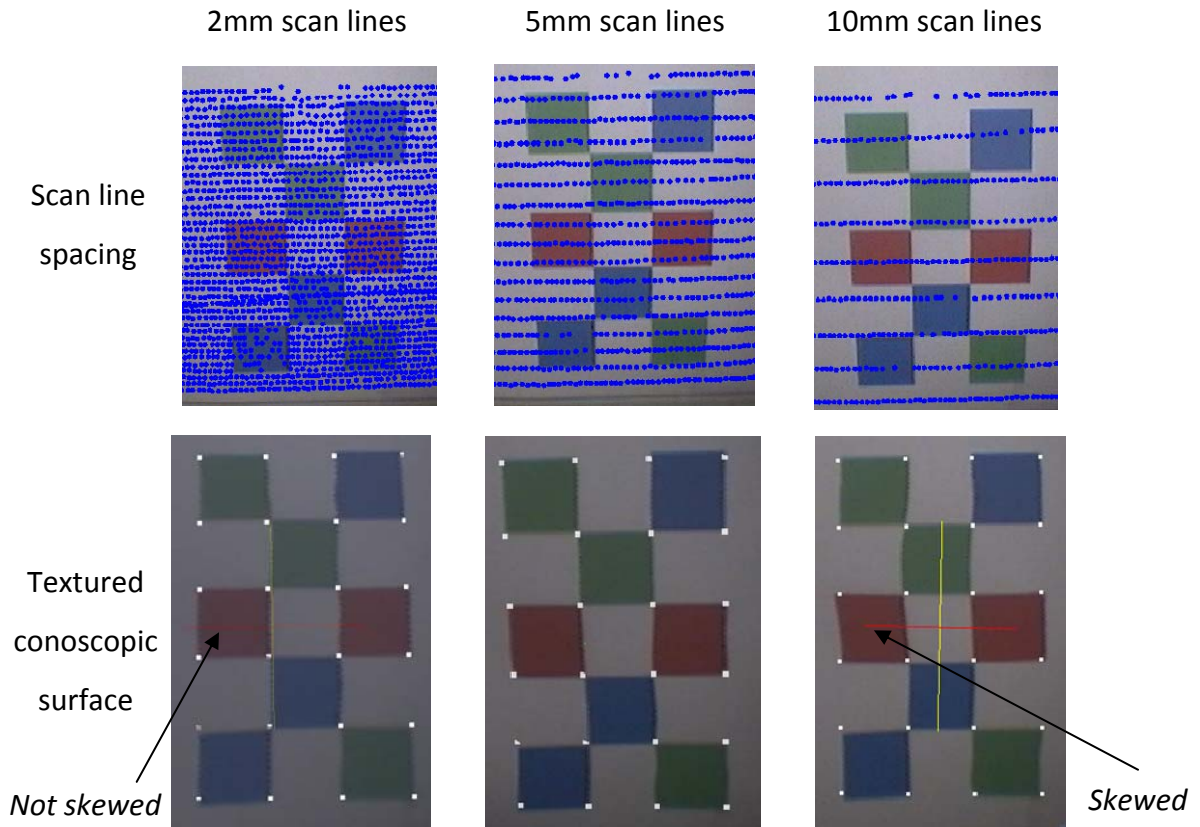
Figure 8. Representative textured surfaces constructed from data taken at 2, 5, and 10mm scan line spacings. Top row: Plots showing the conoscopic line spacings that were used to construct each corresponding textured surface in the lower row. The blue dots represent the 3D points obtained by the conoscope. Bottom row: Textured conoscopic surfaces displayed with white dots representing actual locations of square corners. The black arrows points to a skewed square constructed from the 10 mm line spacing that is not skewed in the 2mm line spacing.

b. Ex-vivo porcine kidney

i. Validation using probe-localized points

The textured surfaces constructed from ex-vivo porcine kidneys were found to have submillimetric accuracy over the 10 trials performed (Table 3). The mean leave-one-out TRE and FRE over all trials was calculated to be 0.99 and 0.78 mm, respectively. The qualitative results can be seen in Figure 10.

Table 3. Accuracy of the conoscopic textured surfaces from ex-vivo porcine kidneys. The TRE and FRE of the point-based registrations between the gold-standard probe-localized fiducials and the texture-localized fiducials are shown.

| | TRE (leave-one-out) (mm) | | | | FRE (mm) | Nbr. of |
Trial	Mean	Std	Max	Min	Mean	Fiducials
1	0.56	0.25	1.05	0.10	0.45	10
2	0.70	0.31	1.09	0.14	0.56	10
3	1.14	0.76	3.04	0.42	0.96	10
4	0.76	0.45	1.55	0.16	0.62	10
5	0.82	0.30	1.39	0.37	0.62	9
6	0.80	0.39	1.33	0.19	0.66	9
7	1.33	0.98	3.11	0.32	1.05	9
8	1.40	0.82	3.26	0.58	0.99	11
9	1.05	0.40	1.85	0.45	0.77	11
10	1.33	0.77	2.85	0.41	1.08	5
All	0.99				0.78	
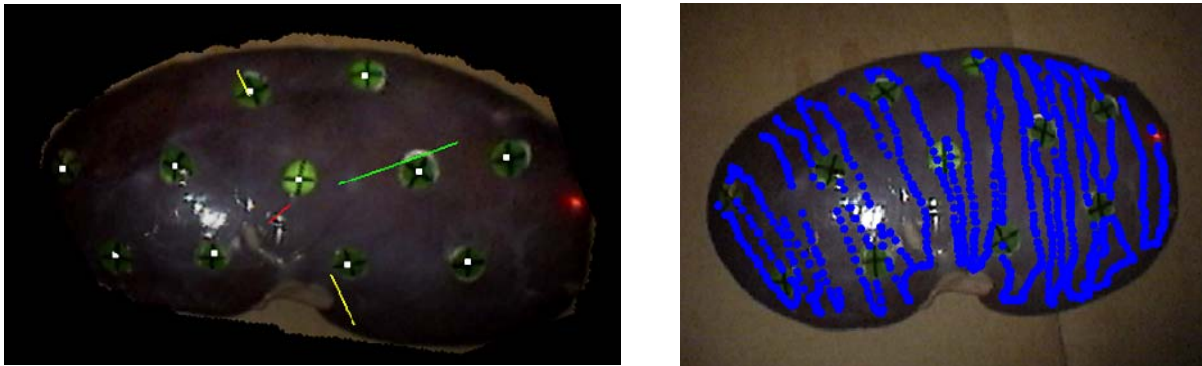
Figure 10. Left: Textured conoscopic surface of ex-vivo pig kidney covered in fiducials with white dots representing the true fiducial locations. Right: the conoscopic points (blue dots) that were used to construct the surface.

ii. Comparison to LRS

While the previous studies validated the conoscopic texture using probe-localized points, a comparison to an LRS texture showed a submillimetric mean TRE and FRE over 5 trials (Table 4). While a total of 10 fiducials were used, small portions of some surfaces were not constructable as the Polaris went out of range. Therefore, in some cases, the fiducials in the small unconstructable areas were not able to be used. One representative result in Figure 11

shows the LRS surface overlaid on the conoscopic surface. The small amount of error is
apparent as shown by the white dots representing the conoscopic fiducial centers align quite
well with the LRS surface.

Table 4. Comparison between LRS and conoscopic surface textures. The leave-one-out TRE and FRE calculated
between fiducials localized in the LRS and conoscopic textures are shown.

	TRE (leave-one-out) (mm)				FRE (mm)	Nbr. of
Trial	Mean	Std	Max	Min	Mean	fiducials
1	0.53	0.33	1.28	0.23	0.43	10
2	0.48	0.17	0.73	0.24	0.38	9
3	1.05	0.42	2.13	0.63	0.84	10
4	0.58	0.30	0.96	0.16	0.44	8
5	0.98	0.46	1.61	0.29	0.76	10
All	0.73				0.57	
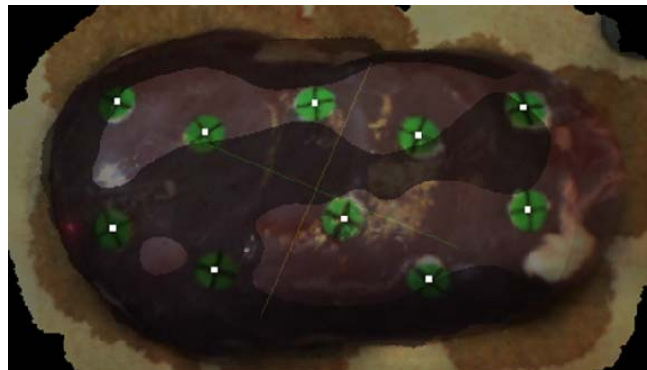
Figure 11. LRS surface overlaid on conoscopic surface. White dots represent conocopic fiducial centers.

c. Ex-vivo human cadaver kidney

To verify the accuracy of the conoscopic texturing method on a human kidney, a point-
based registration was performed between the fiducial stickers localized in the textured surface
and those localized using a Polaris probe. The results are shown below in Table 5 and Figure 12.

The mean leave-one-out TRE over 4 trials was found to be 0.88 mm, with a maximum not exceeding 1.5 mm.

Table 5. Accuracy of the conoscopic textured surfaces taken from an ex-vivo kidney from a human cadaver.

	TRE (leave-one-out) (mm)				FRE (mm)
Trial	Mean	Std	Max	Min	Mean
1	0.93	0.40	1.43	0.35	0.64
2	0.93	0.21	1.13	0.60	0.53
3	0.82	0.24	1.09	0.54	0.53
4	0.86	0.24	1.25	0.53	0.53
All	0.88				0.56
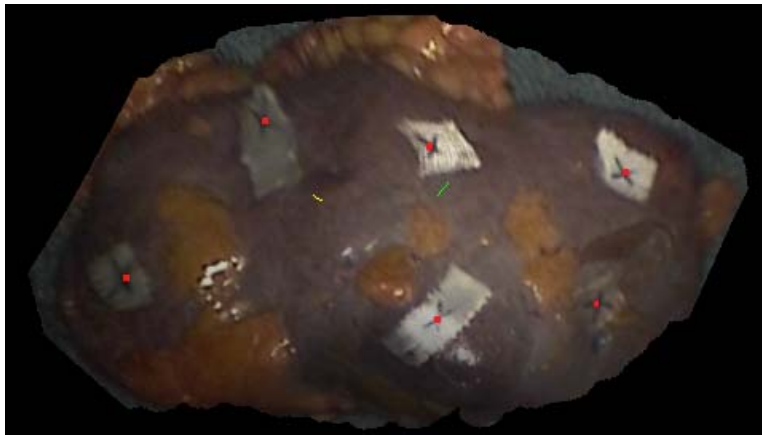
Figure 12. Textured conoscopic surface of the ex-vivo human cadaver kidney. The white stickers marked with an "x" are the fiducials, and the red dots represent the gold standard Polaris-localized positions.

d. Scanning and post-processing times

The mean scan time for 10 porcine and 4 human cadaver cases was found to be 56 +/- 9 s, while the mean post-processing time for the MATLAB and Python scripts was 35 +/- 9 s. The total scan and post-processing time per case was found to be about a minute and a half.

Table 6. Scanning and post-processing times for 10 porcine and 4 human cadaver cases. The post-processing step consists of a MATLAB and python script.

Trial	Scan Time (s)	Running Time (s) MATLAB	Python	Total time (s)
1	62	43.66	1.89	107.56
2	52	37.52	4.02	93.54
3	68	49.89	4.50	122.39
4	51	37.38	1.78	90.16
5	54	26.65	2.15	82.79
6	53	27.61	5.20	85.81
7	53	28.67	6.62	88.30
8	39	19.41	1.67	60.07
9	67	34.15	5.66	106.81
10	69	35.44	5.58	110.02
11	54	28.27	1.31	83.58
12	63	30.30	1.59	94.88
13	51	25.29	1.65	77.94
14	47	24.31	1.61	72.91
Mean	55.93	32.04	3.23	91.20
Std	8.69	8.18	1.92	16.42

Discussion

Significance

In this work, we have presented a novel method of obtaining a textured surface using a conoscope. We believe this method has the potential to track the intraoperative movement of the kidney during laparoscopic surgery, one of the largest challenges in developing abdominal image guidance. While a previous study showed how a geometric surface could be constructed from a tracked conoscopic scan [13], this work's novel contribution shows how to texture-map that surface. This is important because it will allow surface features of the kidney or other abdominal organs to be tracked intra-operatively.

Feature-based registration provides many benefits over surface-based methods such as ICP and intensity-based methods that rely on multiple image acquisitions.   While it is possible to use surface-based methods such as ICP to register an intraoperative organ surface to image

space, previous work has indicated that this method may be unreliable for kidney applications for several reasons. First, any surface scanner such as the LRS can only obtain a limited portion of the organ surface that is within its line of sight. The angle of incidence between the laser and the organ surface also limits the surface acquired and often drops the "edges" of the organ not roughly perpendicular to the scanner. In addition to the limited surface acquired, the smooth, uniform shape of the kidney often results in an ICP registration that is not reliable.

In addition to enabling surface feature tracking, our intraoperative surface acquisition method has the benefit over other imaging modalities of not requiring multiple exposures to radiation, not being subject to the different speeds of sound through tissue, yielding 3D information, and not being prohibitively expensive. Unlike the LRS, it is small enough to fit through a laparoscopic port and can be used minimally invasively. In addition, we believe that this method has the potential to account for non-rigid deformation of the kidney or other abdominal organs during surgery.

Calibration

Because the synchronization of the Polaris, conoscopic, and video streams is so important, the series of tests described in this paper were performed to quantify the accuracy of the synchronization. Characterizing the synchronization error is important for several reasons. First, it is important to detect if there is any offset or drift in the data streams so we can correct for it. Once any offset or drift is corrected, the final synchronization accuracy will place a limit on the accuracy of the texture map as well as the conoscope scanning speed (see Table). For instance, larger errors in the synchronization can be offset by moving the conoscope across the targeted object at a slower speed. Finally, knowing the synchronization error will help us determine what frame rates we need in future improvements if a certain scan speed or accuracy is desired.

Table 7. Expected texture error for different scan speeds, calculated for a Polaris frame rate of 60 Hz and assuming Polaris timing is off by 1 frame.

Scan speed (mm/s)	Expected texture error (mm) per frame of Polaris error
20	0.33
40	0.67
60	1.00
80	1.33

In this work, two tests were performed. The first used an external event, namely a falling object, to block all three data streams simultaneously. To find the synchronization error, the differences between the recorded times of the event in each data stream were calculated. The results showed that the Polaris data stream lagged behind the conoscope by about 30 +/- 13 ms. As the Polaris was running at about 60 Hz, the error is equivalent to about 1.8 Polaris frames.

However, this test is subject to error in the physical setup of the experiment. Although every effort was made to position the laser and Polaris rigid bodies such that they were simultaneously occluded, it is possible that the Polaris delays are a result of the positioning rather than an actual delay. However, several other observations support our findings. First, in a previous study [13] that used an independent method of data collection, a delay of about 2 Polaris frames was also found. Second, Northern Digital, the makers of the Polaris, confirmed that a 20-50 ms delay can be expected between the data request and actual delivery. This is consistent with the results of our study. Finally, we found that adding an offset of 20-25 ms to the Polaris data results in optimal textured surface constructions.

The second synchronization test aimed to test whether there was a bias in the internal video timing. Our tests found a negliable error (-0.4 ms +/- 5.4 ms) that was well within the accuracy of the Windows timing classes, which typically have an accuracy between 10-16 ms [15].

Factors that affect accuracy

In the robot calibration studies described in this paper, we investigated the effects of scan line density on textured surface accuracy. In the image calibration study, we found

submillimetric mean errors for all scan line densities. While we found slightly lower errors for denser line spacings, the difference was not found to be significant. However, since the robot calibration study was performed on a flat image, the accuracy of this method needed to be assessed using a more realistic geometry. While the scan line density did not have as large an effect on texture accuracy for a flat plane, it may if a more convex object is used.

In addition to the geometry, the texture accuracy was evaluated on a more realistic material, namely ex-vivo pig kidneys. The error was calculated using three different gold standards to localize the fiducials: Polaris probe, conoscope, and LRS. While none of the gold standards are perfect, the mean leave-one-out TRE are consistently low and under 1 mm. The submillimetric FRE indicates that the texture is not being distorted compared to the gold standards.

Another factor that we have observed to affect the textured surface accuracy was the proximity of the fiducial targets to the scan boundaries. The accuracy may degrade at edges if the points to interpolate from are scare and the curvature is high. Depending on the interpolation settings, the features at the edge may "bleed" outwards (Figure 13).

Figure 13. Examples showing the potential inaccuracy of the textured surface at the edges, due to the lack of interpolating points near the high curvature area and "bleeding out" of the texture.   The red arrow shows the fiducial close to the edge that was distorted due to the lack of points.

Another factor that impacts textured surface accuracy is the optical tracking accuracy. Because the optically tracked target is attached to the conoscope body, while the measurement taken by the laser can range from 15-25 cm away, the "lever arm" effect can cause small errors

45

in the optical tracking to be magnified at the measurement site. Future work to improve texture accuracy could focus on improving optical tracking, for example, by moving from a passive to an active infrared tracking system.

In addition, the parameters that control the segmentation of the laser dot from the video images, construction, and clipping of the textured surface can be manually fine-tuned to produce an optimal result. In future work, an optimization algorithm could be developed to automatically choose these parameters, possibly using a cost function based on an expected surface feature shape.

Future improvements to the method could also focus on the segmentation of the laser dot. Currently, a simple difference image and threshold are used to track the laser dot. However, in a more realistic laparoscopic environment, further enhancements to the algorithm may be needed to address slight kidney movements, small changes in lighting, and the movement of the conoscopic tube attachment or instruments in the video frame.

While our system is currently not set up to immediately process all the data after acquisition, this is a step that should not be difficult to achieve. Currently, a manual scan of a kidney takes an average of 55 seconds. The post-processing step running times take about 30 seconds and could be decreased if the scripts were implemented in C++ and tailored for speed. Increasing the video and Polaris frame rates could allow the conoscope scan speeds to increase, enabling a decrease in the acquisition time or increase in scan line density. The main challenge to decreasing post-processing time would be to automate the algorithm parameter selections. Either an optimization as discussed above or a parameter selection tailored to the specific laparoscope and lighting conditions could be used to achieve automation.

Future work

While we have presented a novel conoscopic texture-mapping method and reported its accuracy, the next step is to investigate using this method for intraoperative image guidance. This will involve several steps. First, the feasibility and accuracy of this method should be demonstrated in a laparoscopic setting. This will probably be most convenient to do using a porcine model. Second, a full registration accuracy study should be performed to investigate

(a) the accuracy of an image volume to conoscopic surface registration and (b) the accuracy of a feature-tracking registration using the conoscopic surface to account for intraoperative kidney motion. Third, a registration method to correct for possible non-rigid kidney deformation should be explored. This method could be spline or model-based and incorporate the features tracked in the conoscopic textured surface.

In addition to registration studies, the interaction between the conoscopic laser and in vivo kidney tissue should be investigated. We have observed that in vivo tissue has different reflective properties than ex-vivo, resulting in a different signal to noise ratio. Also, different organs seem to have their own individual properties. These tissue properties may require different laser properties, such as power and frequency, tailored to each application.

Finally, a mechanical design to automatically scan the conoscope across the target organ should be developed. The reason is that a steady, automated scanning motion would prevent sharp jumps in speed that would affect the texture accuracy. Also, automated scanning would be more convenient for a surgeon or technician than manually aiming the conoscope across the target organ.

Once these matters have been investigated, we would like to pursue clinical trials. A sterilizable attachment has already been developed to allow clinical usage. The ultimate goal would be to incorporate image guidance into robotic and laparoscopic partial nephrectomies. With further studies and improvements discussed in this paper, we believe this could be an exciting and achievable goal.

Conclusion

In this paper, we have presented a novel method for texture-mapping a 3D surface obtained by a conoscopic laser. Calibration and accuracy studies were performed using phantoms and ex-vivo porcine kidneys covered with surface fiducials. The results showed that the textured surfaces could be reconstructed with submillimetric mean registration errors. These promising results indicate that it may be feasible to use the conoscopic textured surfaces to track intraoperative kidney motion for use in minimally invasive image guidance.

References

[1]   Becker, F., et al., *Elective nephron sparing surgery should become standard treatment for small unilateral renal cell carcinoma: Long-term survival data of 216 patients.* Eur Urol, 2006. **49**(2): p. 308-13.

[2]   Dunn, M.D., et al., *Laparoscopic versus open radical nephrectomy: a 9-year experience.* J Urol, 2000. **164**(4): p. 1153-9.

[3]   Benway, B.M. and S.B. Bhayani, *Robot-assisted partial nephrectomy: evolution and recent advances.* Curr Opin Urol. **20**(2): p. 119-24.

[4]   Scoll, B.J., et al., *Robot-assisted partial nephrectomy: a large single-institutional experience.* Urology. **75**(6): p. 1328-34.

[5]   Kos, S., et al., *MR-guided endovascular interventions: a comprehensive review on techniques and applications.* European Radiology, 2008. **18**(4): p. 645-657.

[6]   Peters, T. and K. Cleary, eds. *Image-Guided Interventions*. 2008, Springer: New York. 557.

[7]   Ding, S., et al., *Semiautomatic registration of pre- and postbrain tumor resection laser range data: method and validation.* IEEE Trans Biomed Eng, 2009. **56**(3): p. 770-80.

[8]   Dumpuri, P., et al., *Model-updated image-guided liver surgery: preliminary results using surface characterization.* Prog Biophys Mol Biol. **103**(2-3): p. 197-207.

[9]   Clements, L.W., et al., *Robust surface registration using salient anatomical features for image-guided liver surgery: algorithm and validation.* Med Phys, 2008. **35**(6): p. 2528-40.

[10]   Sirat, G.Y., *Conoscopic Holography .1. Basic Principles and Physical Basis.* Journal of the Optical Society of America a-Optics Image Science and Vision, 1992. **9**(1): p. 70-83.

[11]   Sirat, G.Y. and D. Psaltis, *Conoscopic Holograms.* Optics Communications, 1988. **65**(4): p. 243-249.

[12]   Danilchenko, A., *Doctoral Dissertation: Fiducial-Based Registration with Anisotropic Localization Error.* Vanderbilt University, 2011.

[13]   Burgner, J., Simpson, A. L., Fitzpatrick, J. M., Lathrop, R. A., Herrell, S. D., Miga, M. I., and Webster, R. J. III, Conoscopic Holography for Intraoperative Digitization:

Characterization and Application for Registration. (Submitted to International Journal of Medical Robotics and Computer Assisted Surgery, Dec. 2011.)

[14]   Simpson, A.L., Burgner J., Glisson, C. L., Pheiffer, T.S., Herrell, S.D., Webster, R. J. III, Miga, M. I. A Comparison Study of Contact and Non-Contact Surface Acquisition Methods with Application to Image-Guided Interventions. (Submitted to IEEE Transactions on Biomedical Engineering, Nov. 2011.)

[15]   "GetTickCount function" Microsoft Developer Network. Retrieved 2/26/12 from msdn.microsoft.com/en-us/library/windows/desktop/ms724408(v=vs.85).aspx

CHAPTER 4

INTRA-OPERATIVE REGISTRATION FOR MINIMALLY INVASIVE KIDNEY SURGERY USING

TEXTURED CONOSCOPIC SURFACES

Introduction

Minimally invasive surgery is growing in popularity for the surgical treatment of kidney cancer. The advantages of this method over open approaches include reduced scarring and faster recovery times [7-8]. However, minimally invasive surgery presents greater challenges for the surgeon because it requires greater surgical dexterity. In addition, because the surgery is performed in small, enclosed, unevenly-illuminated cavities, it is more difficult for surgeons to visualize structures and orient themselves, and the manipulation of multiple surgical instruments in small spaces is challenging. Robotics has facilitated greater usage of minimally invasive surgery, as it allows for finer control of tools through small ports [9-10]. Incorporating image guidance into minimally invasive surgery could provide further benefits by allowing surgeons to more easily orient themselves, visualize tumor margins, and avoid critical healthy structures such as vessels.

While much progress has been made in the field of surgical navigation, one of the central challenges for developing soft tissue guidance is the movement and deformation the organ may undergo during the surgery. To track this deformation, different methods using ultrasound, intraoperative CT, bi-planar fluoroscopy, laparoscopic camera, electromagnetic tracking, and intraoperative MR have been explored. However, each has its limitations: ultrasound has limited imaging capabilities, signal to noise, measurement challenges due to velocity changes through tissue, laparoscopic camera and fluoroscopy provide only 2D images which can be difficult to use for navigation, intraoperative CT and fluoroscopy involve radiation exposure to patient and surgeon, intraoperative MR requires an MR-compatible operating suite and has patient access challenges [11], and electromagnetic tracking can be limited by a small tracking volume [12].

To overcome these challenges, intra-operative laser scanning of the organ surface can be used to track organ motion. A laser range scanner (LRS) has been used in previous applications to account for organ motion and deformation [13-15]. However, the LRS cannot be used in minimally invasive surgeries due to its large size. Moreover, the stereoscopic triangulation method it uses to calculate distances makes miniaturization difficult, as a minimum intraocular distance must be maintained to obtain accurate measurements.

In previous work, a laser-scanning method that can be used minimally invasively was developed [1]. This method uses conoscopic holography, which measures the distance to an object at a single point using phase changes and interference patterns from the reflected light [16-17]. Unlike the LRS, which uses a stereoscopic method to calculate distance, the conoscopic laser can be made small enough to fit through a trocar port. When optically tracked, the conoscopic can be swept across an organ surface to obtain a 3D point cloud. The accuracy of the conoscopic surfaces reconstructed from this method is described in [1].

Registration of intra-operative conoscopic surfaces to pre-operative images for the purpose of image guidance can be achieved using surface-based methods; however these methods often have higher error than would be desirable. The accuracy of surface-based registrations of conoscopic surfaces was explored in [1, 5]. High TRE was found for ICP registration of conoscopic kidney phantom surfaces in [1], with a mean TRE of 3.2 mm for 5 trials.

One reason surface-based registration methods are not reliable is the lack of distinctive geometric surface features in the kidney. In addition, the conoscope can only scan the visible kidney surface in its line of sight, and minimally invasive conditions may further limit the kidney surface scanned. The lack of high-curvature surface areas and the limitation in the scanned area both contribute to potential inaccuracy when using surface-based registration methods for the kidney.

Because of the high error associated with surface-based registration methods, better registration methods are needed. Incorporating texture-mapping could improve intra-operative registration, as it would allow features from the texture map to be tracked.

In the previous chapter, we developed a novel method for texture-mapping conoscopic surfaces, with the goal of using the texture map for intra-operative feature tracking and registration. In that method, a tracked conoscopic laser was swept over an organ to obtain a surface point cloud. Synchronized laparoscopic video was then used to texture-map the organ surface. The accuracy of the texture-mapping method was evaluated using phantoms, ex-vivo pig kidneys, and ex-vivo human cadaver kidneys. The results were shown to be quite promising, and the mean error was consistently found to be below 1mm.

While the previous chapter presented the conoscopic texture-mapping algorithm and evaluated its accuracy, the goal of this chapter was to evaluate the feasibility of using intra-operative conoscopic textured surfaces for laparoscopic guidance.

Although conoscopic surfaces can be used to track intra-operative kidney movement, this method alone is not sufficient for image guidance: a method to register conoscopic to image space is still required. While previous work has explored using surface-based registration to align intra-operative surfaces with image space, this method is not reliable in the kidney for the reasons described above. To overcome this gap, we propose using an initial intra-operative CT or 3D fluoroscopy scan after the abdomen is insufflated and the kidney is isolated from the surrounding tissue. (Intra-operative CT and 3D fluoroscopy both provide 3D images using X-rays; however, we define 3D fluoroscopy to be the scanning method that uses cone-beam CT and flat panel detectors and does not move the patient or scanner along the axial direction.) In this method, an intra-operative CT or 3D fluoroscopy scan of the isolated kidney is used to register image to conoscopic space. There are multiple ways this could be done. First, radio-opaque fiducials could be attached to the kidney surface and localized in both intra-operative image and conoscopic scans. A point-based registration could then align the image and conoscopic spaces. Second, the intraoperative CT or 3D fluoroscopic scanner could be tracked in the same space as the conoscope, and a calibrated transformation would enable an image to conoscopic space registration.

Ultimately, the intra-operative image could be registered to the pre-operative for better navigation. Using one of the intra-operative image to conoscopic registrations described above, the pre-operative image could then be registered to conoscopic space. The advantage

of using the intra-operative CT or 3D fluoroscopy scan in an additional registration step is that more information about the entire kidney is available. Instead of using only partial conoscopoic surface information, which necessitates an unreliable surface-based registration, now the whole kidney image is available for registration. While this is the ultimate goal, here I limit the study to an evaluation of the intra-operative image to conoscopic scan registration.

In this chapter, I present a method for laparoscopic guidance using an initial intraoperative 3D fluoroscopic scan and successive textured conoscopic scans to account for organ movement during surgery. In this method, features localized from the conoscopic surface textures before and after movement are aligned using a point-based registration. The accuracy of this registration method is evaluated in live, anesthetized swine using a laparoscopic surgical approach.

Methods

A. Surgical procedure

The surgical procedure described here uses an intra-operative 3D fluoroscopic scan and conosopic surface scans to provide minimally invasive image guidance for the kidney (Figure 1). The general method will be outlined in this section, while the specific details for the experiment we performed are described in Section F. The surgical procedure followed has the following steps:

1. Inssufflate abdomen and insert laparoscopic trocar ports.
2. Position surface fiducials on kidney. These fiducials could be either physical objects attached to the surface of the kidney or marks placed on the kidney. For the purposes of validation, internal fiducials can also be inserted into the kidney parenchyma to serve as targets.
3. Obtain initial intra-operative 3D fluoroscopic scan. Because the abdomen is filled with gas, there is good contrast for the visible top kidney surface. As a model for human surgery, pigs provide kidneys which resemble human kidneys in size and morphology.

However pigs lack the encompassing perirenal fat that humans have. To make the pig more closely resemble humans, padding is added to provide contrast.

4. Obtain a texture-mapped conoscopic scan (Figure 2). The conoscopic scanning procedure will be described in Section B.

B. Conoscopic scanning procedure

The goal of this step is to sweep a tracked conoscopic laser across the kidney surface to obtain a surface point cloud, and to color-map it using synchronized laparoscopic video. As the color-mapping method requires the red laser dot in each video frame to be tracked, we simplify the image processing by fixing the laparoscope and turning off the laparoscopic lights. The image processing involved in tracking the red dot is much less complicated without the ambient light.

In our experiment, the following was done under breath hold. When the scan was ready to be taken, steps 2-4 can be semi-automated to take only 1-2 seconds.

1. Fix the laparoscope. In future improvements, the laparoscope could also be tracked, allowing it to move; however, for the sake of simplicity, it was fixed in this experiment. In addition, this requirement may not be clinically onerous, because robotic systems such as the DaVinci often attach the laparoscope to an arm that is trivial to fix.

2. Capture a reference video frame with laparoscopic light on. This will serve as the texture image that will be used to color-map the kidney surface.

3. Turn off laparoscopic lights. As the red laser dot moves across the kidney surface, it is easier to track it in the video feed without the ambient light.

4. Display blended video. Since the laparoscopic light is off, the kidney surface cannot be seen. Blend the laparoscopic video feed, which shows only the position of the red laser dot, with the reference image, which shows the position of the kidney and surroundings. This is done so that the conoscope can be properly swept across the kidney surface.

5. Scan surface with conoscope. Sweep the kidney surface with the optically tracked conoscopic laser. The method and calibration described in [1] will produce a 3D

surface point cloud from synchronized Polaris and conoscopic data. This surface can be
texture-mapped using the technique described in the last chapter, and explained in
greater detail in Section C.

6. Take additional conoscopic scans after the kidney has been moved. To validate the
registration, take an intra-operative 3D flouroscopic scan for each additional
conoscopic scan so that the internal targets can be localized.

C. Texture-mapping algorithm

The method described here texture-maps (i.e. applies the true colors to) a surface
generated by sweeping an optically-tracked conoscopic laser across an organ [1, 5]. The
texture-mapping method matches each surface point to a synchronized laparoscopic video
frame showing the location of the laser dot. The laser dot locations in the video are used to
color-map each point on an organ surface. The texture mapping algorithm has the following
steps (See Figure 3 for an illustrated diagram):

1. Sweep the conoscopic laser across an organ surface. Follow the procedure described in
Section B to fix the laparoscope, record a reference laparoscopic image with the light
on, and then record all further data with the light off.

2. Record and synchronize the optical tracking, conoscopic measurements, and the
standard laparoscopic video feed.

3. To obtain surface point cloud **P**, transform each synchronized conoscopic distance and
optical tracking measurement to yield a 3D point P_i. The details of this transformation
are found in [1].

4. Obtain texture coordinates of each point P_i by finding the location of the red laser dot in
the corresponding video frame F_i. The location of the red laser dot is found calculating
the center of all pixels with a red channel value about threshold K_{red}. The location of the
dot yields the row and column texture coordinates (R_P, C_P) at the points **P**.

For i=1 to length(**P**)
        F_i = GetCorrespondingVideoFrame(P_i)
        [**r c**] = coordinates { RedChannel(F_i) > K_{Red}}
        [R_{Pi} C_{Pi}] = mean([r c]);

end

5. The following thin plate spline equations are used to interpolate the texture coordinates. These equations can be constructed in the form [B] $\bar{x} = \bar{b}$, where B is a m x n matrix containing the weights **W**, **A, and D**; $\bar{x}$ is a n x 1 vector containing the distances from n points [x,y,z] to the control points **P**; and $\bar{b}$ is a n x 1 vector containing the known texture coordinates (**R$_P$**, **C$_P$**) at points **P**. The matrix system of equations for the row and column texture coordinates (**R$_P$**, **C$_P$**) corresponding to points **P** can be solved for the weights **W$_R$** , **W$_C$**, **A$_R$**, **D$_R$**, **A$_C$**, and **D$_C$**:

$$R_P = A_R\,X + D_R + \sum_{i=1}^{length(\mathbf{P})} W_{Ri}\,||\mathbf{P} - \mathbf{P}_i||^2 \ln\left(||\mathbf{P} - \mathbf{P}_i||\right)$$

$$C_P = A_C\,X + D_C + \sum_{i=1}^{length(\mathbf{P})} W_{Ci}\,||\mathbf{P} - \mathbf{P}_i||^2 \ln\left(||\mathbf{P} - \mathbf{P}_i||\right)$$

where **A$_R$** and **A$_c$** are 3x3 matrices describing an affine transformation, **D$_R$** and **D$_C$** are 3x1 vectors describing a constant translation, **W$_R$** and **W$_C$** are 3xN weights describing the non-linear components of the spline, and ||**P**-**P$_i$**|| is the Euclidean distance between points **P** and **P$_i$**. The following constraints are used:

$$\sum_{i=1}^{m=\,length(\mathbf{P})} W_i = 0$$

$$\sum_{i=1}^{m=\,length(\mathbf{P})} W_i P_i = 0$$

6. Use the spline to interpolate the texture coordinates to super-sampled surface points **S**. The color at the points **S** are obtained by looking up the pixel values at texture coordinates (**R$_S$**, **C$_S$**) in the reference laparoscopic image F$_0$, taken with the lights on.

$$S = SupersampleSurface(\mathbf{P})$$

$$R_S = A_R\,X + D_R + \sum_{i=1}^{length(P)} W_{Ri}\,||S - P_i||^2 \ln\left(||S - P_i||\right)$$

$$C_S = A_C\,X + D_C + \sum_{i=1}^{length(P)} W_{Ci}\,||S - P_i||^2 \ln\left(||S - P_i||\right)$$

$$\text{Color}(S) = F_0(R_S, C_S)$$

Because the laparoscope is fixed during the entire scan, and the pig is in breath-hold, all video frames should be in the same space.

D. Registration method

The method to register the intra-operative 3D fluoroscopic scan to optically tracked conoscopic space is described by the following steps:

1. Register the intra-operative 3D fluoroscopic scan space to the optically-tracked conoscopic scan space (Figure 1, steps 2-3). This can be done using a tracked intra-operative fluoroscopic scanner (registration performed using external targets attached to scanner) or by attaching radio-opaque fiducials to the kidney surface. For this experiment, we attached radio-opaque fiducials (4x4mm iodine-soaked, plastic-covered sqaures) to the kidney surface. A point-based registration was used to register the fiducials localized by 3D fluoroscopy to those localized from the conoscopic texture.

2. To account for kidney movement after the initial registration, localize the surface fiducials from the conoscopic textured surfaces obtained before and after the movement (Figure 1, steps 3-4). Register the two surfaces using point-based registration.

1. **Insufflate abdomen, insert ports, and uncover kidney**
   - Attach or mark fiducials on kidney surface
   - For validation in this experiment, insert internal fiducials

2. **Take initial intra-operative CT scan**

Register CT to optically-tracked conoscopic space

3. **Take initial conoscopic scan**

After kidney movement, register conoscopic scans

VALIDATION

5. **Take validation CT scan(s)**
   Use CT-localized internal fiducials to calculate TRE

4. **Take subsequent conoscopic scan(s)**

Register

Figure 1. Surgical procedure for using intra-operative 3D fluoroscopy and conoscopic scanning to provide minimally invasive guidance. Registration steps are shown by the arrows. More details describing the conoscopic scanning procedure are shown in Figure 2.

1. Fix laparoscope

2. Record reference image from laparoscope (with light on)

3. Turn laparoscopic light off so laser dot can be tracked more easily

4. Display reference image blended with laparoscopic video for navigation purposes

5. Scan conoscope over kidney and record laparoscopic video
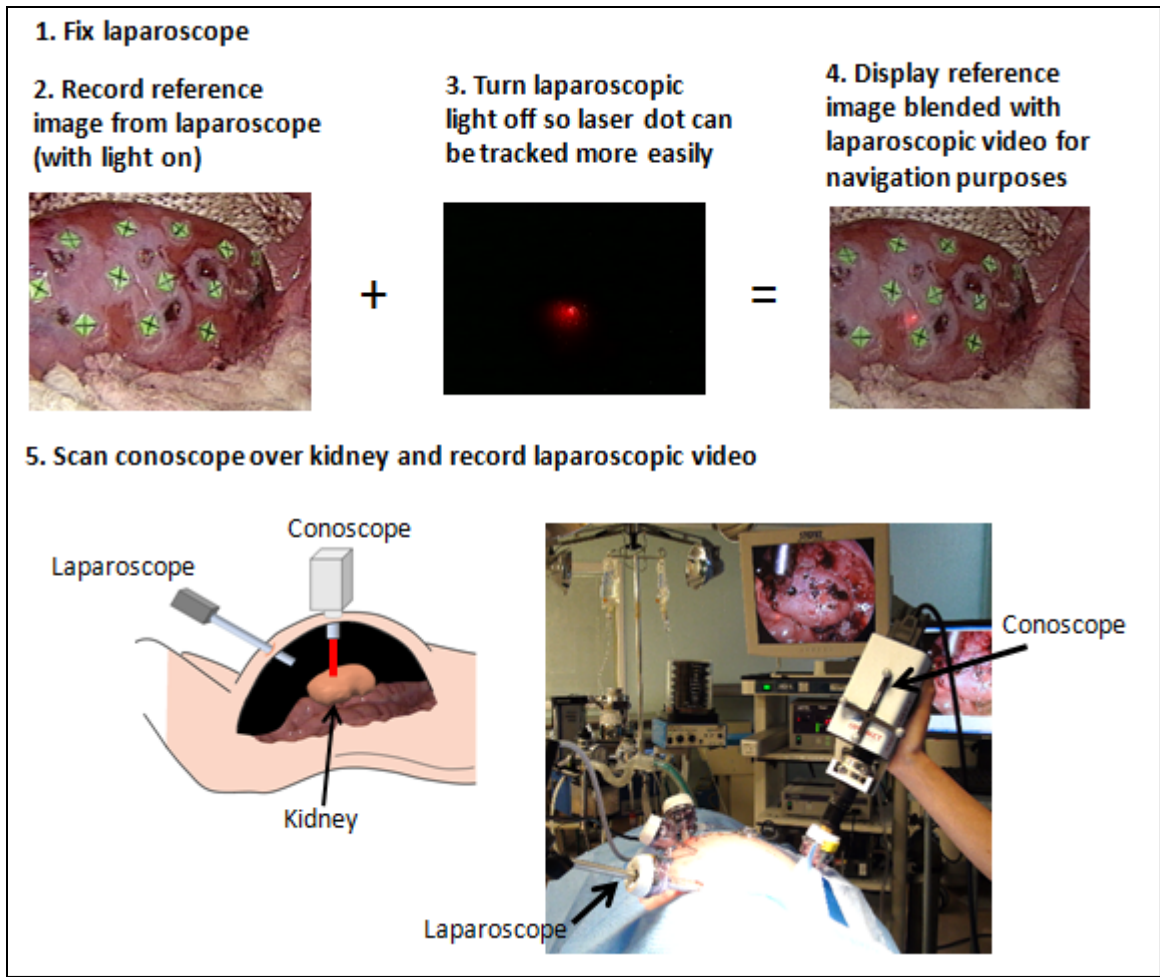
Figure 2. Conoscopic scanning procedure used to obtain textured surface data. See Figure 3 for texture mapping algorithm.

1. **Scan conoscopic across kidney.**
   (Fix laparoscope and record reference image as described in previous section.)

2. **Record and synchronize the following data**

   Optical tracking data (for tracked conoscope)

   Conoscopic distance measurements

   Laparoscopic video
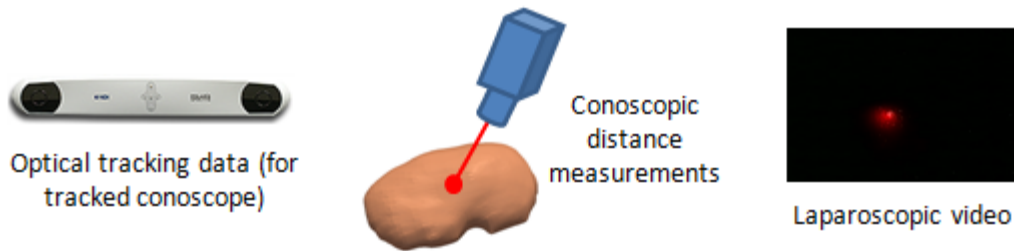
3. **To obtain surface point cloud, transform each synchronized conoscopic and optical tracking measurement to yield 3D point [1]**
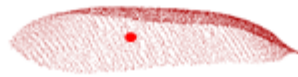
4. **For each conoscopic surface point, find its corresponding video frame**

5. **Find location of red laser dot in each video frame to yield texture coordinates**
   a. Subtract 2 successive frames
   b. Threshold the red channel of the difference image
   c. Calculate centroid of thresholded area

   One laparoscopic video frame

   Y Texture Coordinate

   X Texture Coordinate

   All texture coordinates (blue) plotted over reference frame
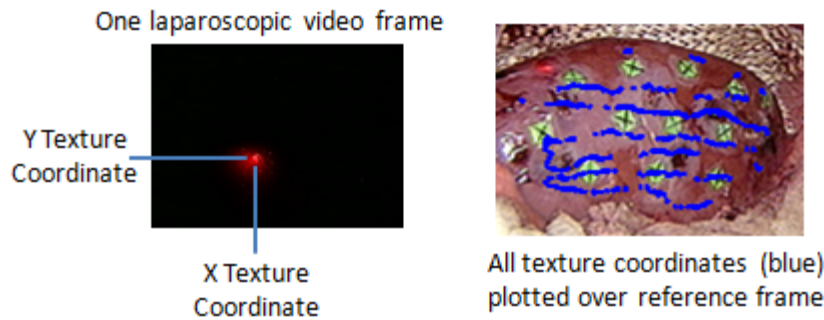
6. **To obtain textured surface, use texture coordinates for each surface point to map reference image to surface point cloud**

   Texture map

   Reference frame   Surface point cloud   Textured surface
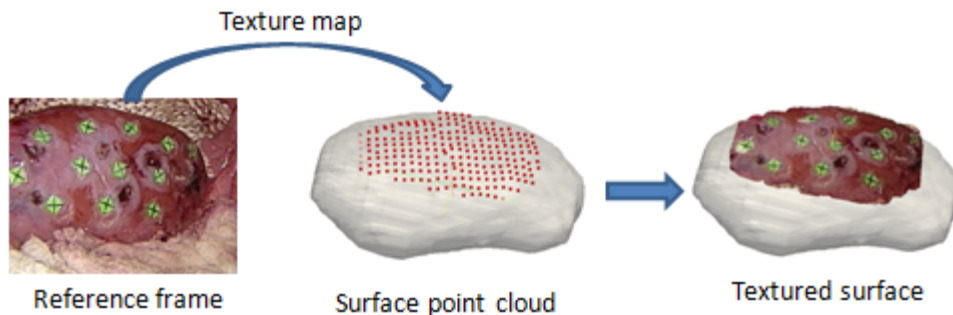
Figure 3. Texture mapping algorithm. See Figure 2 for procedure used to obtain conoscopic data.

E. Experiment

The surgical procedure described above was performed on two live, anesthetized pigs under an IUCAC-approved protocol. Both kidneys were scanned. For each kidney, 3-4 different poses were obtained by moving the kidney and tilting the abdomen at different angles, as is common clinically. For each pose, one O-arm scan and between 1-3 conoscopic scans were taken.

Equipment

For this experiment, the Medtronic O-arm (Louisville, CO) was used to take 3D fluoroscopic images. The image volume was 512 x 512 x 192 voxels, with a voxel size of 0.415 x 0.415 x .833 mm. Scanning was done under 80 kVp and 240 mAs.

An OPTIMET Probe Head Mk3 conoscope (North Andover, MA) was used to scan the kidney. The lens used had an approximate focal range of between 15-20 mm, and the data frequency rate used was 400 Hz.

The conoscope was optically tracked by attaching a Polaris (Northern Digital, Ontario, Canada) passive rigid body to the conoscope body. The calibration used to transform the conoscopic distance measurements to Polaris space is described in [1].

Fiducials

For this experiment, surface fiducials were made using iodine-immersed paper covered in clear plastic. They were attached to the kidney using cyanoacrylate glue, which has been used in other applications to seal vessels and close wounds [2-4]. The fiducials had a size of 4x4mm squares. For the purposes of validation, internal glass bead fiducials (2mm in diameter) were inserted into the kidney parenchyma to serve as targets.

In this experiment, the fiducials in the O-arm scans were localized by thresholding the intensities, and the centroids of each thresholded area were calculated. For the conoscopic surfaces, the fiducials were manually localized using the texture. Each fiducial was localized 3

times, and the mean position was used. In addition, the precision for the manual localization

was calculated.

Similarly, the surface fiducials in the conoscopic scans were localized manually using the

texture, and the mean position of 3 trials was used.

F. Texture accuracy

To evaluate the textured surface accuracy, we calculated the fiducial registration error

(FRE) between the surface fiducials localized from the 3D fluoroscopic scan and from the

conoscopic texture (Figure 1, steps 2-3). The FRE can be thought of as a measure of the

conoscopic texture distortion, using the 3D fluoroscopic scan as the ground truth. The

conoscopic scans were grouped by kidney pose, and the mean, standard deviation, maximum

and minimum FRE were shown.

G. Point-based registration accuracy

The accuracy of the point-based registration method described in Section D was

assessed using the following metrics:

(1) TRE measuring the total registration error internally in the parenchyma (step 5 of

Figure 1). After the registration described in Section D (Figure 1, steps 2-5), the internal fiducial

locations in the initial O-arm scan were compared to their positions in the validation scan,

yielding the TRE.

(2) FRE measuring the error of the conoscopic registration at the surface (Section D, step

2 and steps 3-4 in Figure 1). After kidney movement, the initial conoscopic scan was registered

to the subsequent using surface fiducials. The FRE of this registration is a measure of the

surface registration error, comprised of both texture error and non-rigid deformation.

H. Surface-based registration accuracy comparison

The point-based registration method described takes advantage of the texturing of the

conoscopic surface, from which the surface fiducials are localized. For comparison, this method

was compared to a standard surface-based ICP that does not use texturing. For this

assessment, the TRE was calculated at both the internal and surface fiducials, as neither set was involved in the registration.

I. Measuring Non-Rigid Deformation

The amount of non-rigid deformation encountered while moving the kidney was calculated using the internal and external fiducials. These were localized in the initial and subsequent scans, registered using point-based methods, and the resulting FRE was used as a measure of deformation.

Results

Texture accuracy

The distortion of the conoscopic textured surface was calculated by registering the surface fiducials localized from the conoscopic texture to those from the O-arm. A point-based registration was used, and the FRE is reported in Table 1. A histogram of the error is shown in Figure 4, and an example registration is shown in Figure 5. Because no movement occurred between the O-arm and conoscopic texture scans (Steps 2-3 in Figure 1), the FRE reflects the distortion of the conoscopic texture.

The closest distance between the conoscopic textured surface and the registered O-arm surface is also shown in Table 1.

Table 1. The conoscopic texture distortion. The FRE was calculated between the fiducials localized from conoscopic texture and O-arm scans of the same kidney pose. This also represents the error of the first step of the registration process (Figure 1, steps 2-3).

Kidney	Pose	Trials	FRE (mm)				Closest distance (mm)			
			Mean	Std	Max	Min	Mean	Std	Max	Min
1	1	3	0.9	0.4	2.1	0.3	0.5	0.5	5.0	0.0
	2	3	1.2	0.5	2.3	0.5	0.8	0.9	5.9	0.0
	3	3	1.1	0.4	1.8	0.5	1.1	0.9	4.6	0.0
2	1	3	1.0	0.6	2.4	0.3	1.3	1.4	8.1	0.0
	2	3	0.9	0.2	1.3	0.6	1.1	0.9	6.4	0.0
3	1	3	0.7	0.3	1.5	0.1	0.6	0.5	3.4	0.0
	2	3	0.6	0.3	1.3	0.1	0.8	0.6	3.8	0.0
	3	3	0.8	0.4	2.1	0.2	1.3	0.7	6.7	0.0
4	1	3	1.0	0.4	1.7	0.5	1.1	0.7	3.5	0.0
	2	2	1.0	0.7	2.5	0.2	1.5	0.9	6.3	0.0
	3	3	0.8	0.3	1.5	0.3	1.1	0.8	4.9	0.0
	4	3	0.9	0.5	2.3	0.1	1.0	0.7	4.5	0.0
All		35	0.9	0.4	2.5	0.1	0.9	0.8	8.1	0.0
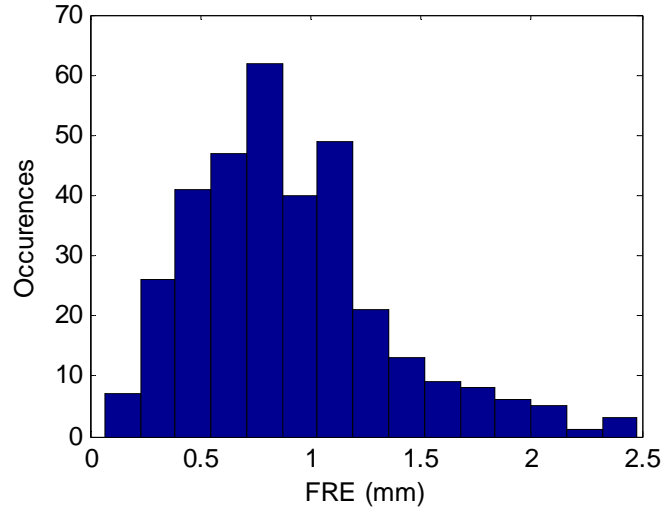
Figure 4. Histogram of conoscopic texture distortion for all 4 kidneys and 35 scans, measured at the surface fiducials. This graph represents the error at all surface fiducials for all trials reported in Table 1.

Figure 5. Registered conoscopic textured surface (Kidney 3, pose 2, scan 1) displayed with true surface fiducial centers (white dots) calculated from O-arm scan. Gray surface indicates segmented kidney surface obtained from O-arm scan.

Point-based registration accuracy

Three measures of the point-based registration accuracy are reported. First, the TRE, measured from the internal fiducials inside the parenchyma, represents the total error for all steps of the registration (Figure 1, steps 2-5). Second, the FRE, measured at the surface fiducials, represents the registration error only between the pre- and post-movement conoscopic surfaces (Figure 1, steps 3-4). Both the TRE and FRE are shown in Table 2 and the error distribution over all scans and fiducials is shown in Figure 4. Finally, the closest distances between the registered pre- and post-movement O-arm surfaces is shown in Table 3.

Table 2. Accuracy of the point-based registration. The TRE measured at internal fiducials represents the total error for all registration steps (Figure 1, steps 2-5). The FRE, measured at the surface fiducials, represents just the error between the pre- and post-movement conoscopic surfaces (Figure 1, steps 3-4).

Kidney	Registration	Trials	TRE (mm)				FRE (mm)			
			Mean	Std	Max	Min	Mean	Std	Max	Min
1	Pose 1 => Pose 2	9	0.3	0.1	0.4	0.1	1.1	0.5	3.3	0.3
	Pose 2 => Pose 3	9	0.2	0.1	0.5	0.1	1.0	0.5	2.6	0.0
	Pose 3 => Pose 1	9	0.4	0.1	0.6	0.3	1.3	0.6	3.9	0.2
2	Pose 1 => Pose 2	9	0.5	0.4	1.6	0.1	0.9	0.4	1.7	0.3
3	Pose 1 => Pose 2	9	0.5	0.2	1.0	0.1	0.8	0.4	1.9	0.2
	Pose 2 => Pose 3	9	0.8	0.4	1.5	0.2	0.9	0.4	1.7	0.2
	Pose 3 => Pose 1	9	1.0	0.5	2.0	0.3	1.0	0.4	2.2	0.1
4	Pose 1 => Pose 2	4	0.5	0.3	1.0	0.2	1.7	0.8	2.9	0.4
	Pose 1 => Pose 3	4	0.9	0.3	1.5	0.5	1.2	0.5	2.5	0.3
	Pose 1 => Pose 4	4	0.8	0.4	1.4	0.1	1.1	0.6	2.7	0.1
	Pose 2 => Pose 3	1	1.0	0.3	1.4	0.5	1.6	0.8	3.7	0.7
	Pose 2 => Pose 4	1	1.0	0.5	1.7	0.2	1.7	0.8	4.1	0.3
	Pose 3 => Pose 4	9	0.7	0.2	1.2	0.4	0.8	0.3	1.4	0.2
	All	86	0.6	0.4	2.0	0.1	1.1	0.5	4.1	0.0
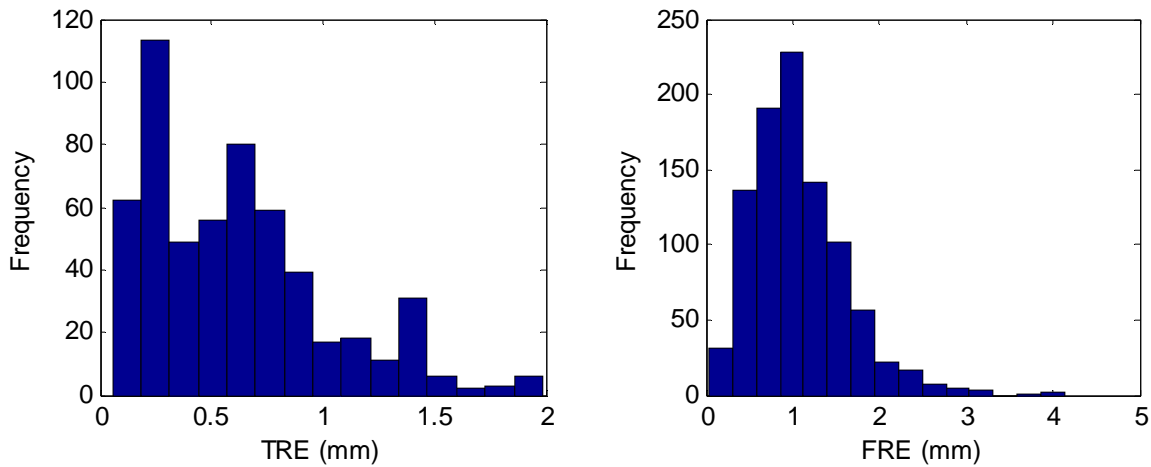
Figure 5. Histograms of point-based registration error over all kidneys, trials, and fiducials. The left graph shows the distribution of TRE measured at internal fiducials, while the right graph shows the FRE measured at the surface fiducials.

Table 3. Closest distance error between the pre- and post-movement O-arm surfaces aligned using the point-based registration.

Kidney	Registration	Trials	Closest distance (mm)			
			Mean	Std	Max	Min
1	Pose 1 => Pose 2	9	0.3	0.2	2.3	0.0
	Pose 2 => Pose 3	9	0.7	0.3	1.8	0.0
	Pose 3 => Pose 1	9	0.7	0.4	2.1	0.0
2	Pose 1 => Pose 2	9	0.5	0.4	1.7	0.0
3	Pose 1 => Pose 2	9	0.7	0.4	2.5	0.0
	Pose 2 => Pose 3	9	0.8	0.5	2.7	0.0
	Pose 3 => Pose 1	9	0.9	0.5	2.8	0.0
4	Pose 1 => Pose 2	4	0.6	0.4	1.6	0.0
	Pose 1 => Pose 3	4	0.4	0.3	1.8	0.0
	Pose 1 => Pose 4	4	0.5	0.4	2.1	0.0
	Pose 2 => Pose 3	1	0.6	0.4	2.0	0.0
	Pose 2 => Pose 4	1	0.7	0.5	2.0	0.0
	Pose 3 => Pose 4	9	0.4	0.3	1.8	0.0
	All	86	0.6	0.4	2.8	0.0

Surface-based registration accuracy comparison

The point-based registration method, which utilizes the conoscopic texture, was compared with one that does not utilize texture, namely surface-based ICP. The accuracy of the ICP registration, where 10 randomly perturbed initial positions were generated for each conoscopic scan, is reported using three measures. The TRE measured at the internal fiducials and at the surface fiducials, as localized from the O-arm scans, is shown in Table 4. Finally, the closest distances between the registered pre- and post-movement O-arm surfaces is shown in Table 5.

To compare the error distributions of the ICP and the point-based registrations, their TRE histograms are shown in Figure 6.

Table 4. Accuracy of surface-based ICP method. The TRE at the internal fiducials and at the surface fiducials, as localized from the O-arm scans, is shown. Ten randomly perturbed initial positions were generated for each conoscopic scan.

Kidney		Trials	TRE (internal) (mm)				TRE (surface) (mm)			
			Mean	Std	Max	Min	Mean	Std	Max	Min
1	Pose 1 => Pose 2	30	5.2	2.3	10.5	1.7	9.7	7.1	27.3	2.1
	Pose 2 => Pose 3	30	8.3	3.2	14.9	1.3	15.0	5.6	35.5	8.1
	Pose 3 => Pose 1	30	5.7	2.1	10.5	0.2	6.5	1.9	11.1	1.2
2	Pose 1 => Pose 2	30	7.2	3.1	19.1	1.9	9.8	4.6	24.1	1.3
3	Pose 1 => Pose 2	30	5.7	2.4	10.7	1.1	6.4	2.5	11.9	1.4
	Pose 2 => Pose 3	30	5.2	1.5	10.0	2.4	5.5	1.5	10.8	2.2
	Pose 3 => Pose 1	30	6.2	2.0	13.7	1.1	6.3	2.1	14.2	1.6
4	Pose 1 => Pose 2	30	6.1	3.2	13.8	0.8	7.2	3.8	15.9	0.6
	Pose 1 => Pose 3	30	5.8	1.5	9.5	2.4	6.7	1.5	10.3	3.3
	Pose 1 => Pose 4	30	4.5	1.8	9.8	2.1	4.7	1.8	10.3	1.5
	Pose 2 => Pose 3	20	6.5	2.1	11.7	2.3	7.5	2.3	12.9	1.5
	Pose 2 => Pose 4	20	6.5	2.2	11.4	1.7	6.9	2.5	12.3	1.4
	Pose 3 => Pose 4	30	4.5	1.9	10.7	0.7	5.0	2.2	12.3	0.6
	All	370	5.9	2.6	19.1	0.2	7.9	4.8	35.5	0.6

Table 5. Closest distance error between pre- and post-movement O-arm surfaces registered using ICP.

Kidney	Registration	Trials	Closest distance (mm)			
			Mean	Std	Max	Min
1	Pose 1 => Pose 2	30	0.4	0.4	3.8	0.0
	Pose 2 => Pose 3	30	0.7	0.5	3.7	0.0
	Pose 3 => Pose 1	30	0.5	0.5	3.6	0.0
2	Pose 1 => Pose 2	30	0.8	0.8	7.2	0.0
3	Pose 1 => Pose 2	30	0.5	0.4	3.1	0.0
	Pose 2 => Pose 3	30	0.5	0.4	3.7	0.0
	Pose 3 => Pose 1	30	0.5	0.4	3.4	0.0
4	Pose 1 => Pose 2	30	0.5	0.4	3.0	0.0
	Pose 1 => Pose 3	30	0.8	0.6	4.3	0.0
	Pose 1 => Pose 4	30	0.8	0.6	3.8	0.0
	Pose 2 => Pose 3	20	0.6	0.5	2.8	0.0
	Pose 2 => Pose 4	20	0.6	0.5	2.8	0.0
	Pose 3 => Pose 4	30	0.6	0.5	3.6	0.0
	All	370	0.6	0.5	7.2	0.0
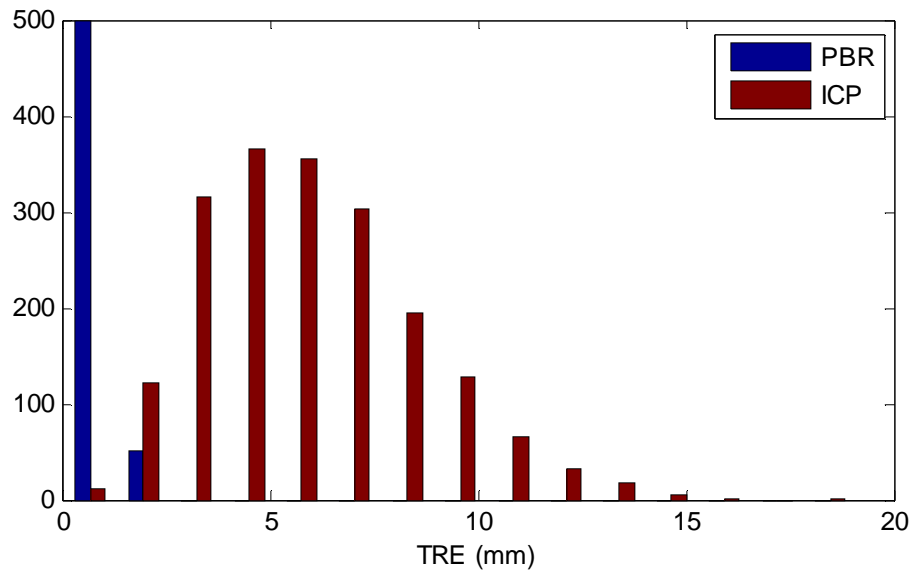
Figure 6. Histogram comparing the TRE between the point-based registration (blue) and the ICP (red). (All kidneys, scans, and fiducials were included in this graph.)

Non-rigid deformation and total error before registration

In order to estimate the movement between kidney poses before any registration was performed, the distance between the fiducial locations in different kidney poses was calculated. In addition, the non-rigid deformation occurring between poses was estimated by the calculating the residual error after a rigid point-based registration was performed. These results are shown in Table 6.

Table 6. Non-rigid deformation and total error before registration between kidney poses, calculated at all surface and internal fiducials localized from O-arm.

Kidney	Registration	Non-rigid deformation (mm)				Total error before registration (mm)			
		Mean	Std	Max	Min	Mean	Std	Max	Min
1	Pose 1 => Pose 2	0.2	0.1	0.6	0.1	15.9	0.2	16.3	15.5
	Pose 2 => Pose 3	0.3	0.1	0.5	0.1	22.7	2.8	27.4	18.1
	Pose 3 => Pose 1	0.4	0.2	1.0	0.1	28.2	2.4	33.1	24.5
2	Pose 1 => Pose 2	0.2	0.1	0.6	0.1	34.1	0.6	34.9	32.8
3	Pose 1 => Pose 2	0.4	0.2	0.6	0.2	11.5	1.1	13.7	9.9
	Pose 2 => Pose 3	0.9	0.4	1.4	0.2	27.9	1.5	30.6	25.5
	Pose 3 => Pose 1	1.0	0.5	1.8	0.1	36.0	2.0	38.6	31.8
4	Pose 1 => Pose 2	0.4	0.2	0.7	0.2	18.0	2.1	21.3	14.9
	Pose 1 => Pose 3	0.9	0.5	1.9	0.2	8.7	1.8	12.0	5.8
	Pose 1 => Pose 4	0.8	0.6	2.3	0.1	31.5	0.9	33.0	30.1
	Pose 2 => Pose 3	1.0	0.4	2.1	0.5	23.0	1.9	26.0	19.6
	Pose 2 => Pose 4	0.9	0.5	2.4	0.1	39.5	2.7	44.5	36.0
	Pose 3 => Pose 4	0.5	0.3	1.1	0.2	23.4	2.5	27.9	19.8
	All	0.5	0.4	2.4	0.1	24.6	8.8	44.5	5.8

Discussion

In these experiments, we have demonstrated the feasibility of intra-operative registration in anesthetized pigs under laparoscopic conditions. This method uses an initial 3D fluoroscopic scan and subsequent textured conoscopic surface scans to account for any ensuing kidney motion. The conoscopic texture provides helpful information that enables surface feature tracking, which yields better results than surface-based registrations that do not take advantage of texture.

Texture accuracy

In this study, the accuracy of the textured surface was estimated by localizing the surface fiducials and comparing them to those localized from the O-arm scan. As no movement occurred between the scans, the point-based FRE reflects any distortions in the conoscopic surface. The results showed a sub-millimetric mean error of 0.9 mm, with a maximum error of

2.5 mm over all 4 kidneys and 35 scans. These results are consistent with the texture accuracy

studies reported in Chapter 3 of this work.

The texture accuracy is lowest at the edges of the conoscopic surface due to

interpolation issues. In Figure 7, we can see that the closest distance after registration is

highest at the edges, where the conoscopic surface is most inaccurate. With a better

interpolation scheme, most of this distortion should be avoided.
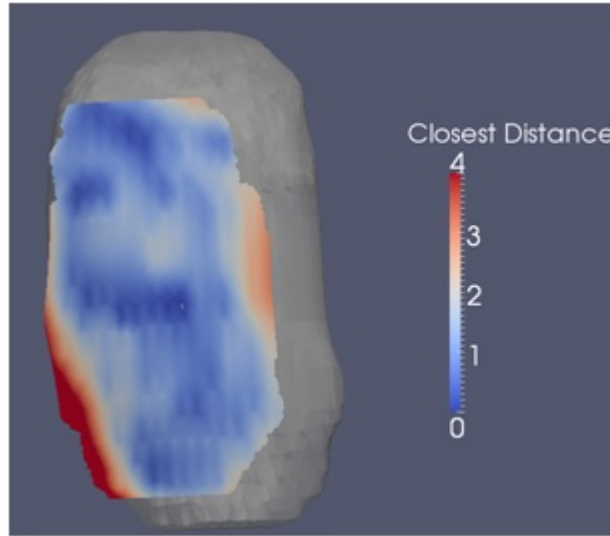
Figure 7. The closest distances between the registered conoscopic surface and the O-arm surface. The surface is
most inaccurate at the edges due to inaccuracies with the interpolation.

Point-based registration accuracy

As there were multiple steps in the point-based registration (Figure 1), we tried to

quantify the accuracy of different steps. There were two main error measures: (1) the total

error for the entire registration method, measured by the TRE at the internal fiducials and (2)

the error of just the conoscopic surface registration (Figure 1, steps 3-4), measured by the FRE

at the surface fiducials.

The results of the point-based registration were quite promising, as they showed a sub-

millimetric mean TRE of 0.6 mm, with maximum error of 2.0 mm over 4 kidneys. The FRE was

higher, with a mean of 1.1 mm and max of 4.1 mm, probably due to the distortion of the

conoscopic surface, especially at the edges. It is likely that the FRE is higher than the TRE

because of a few higher error fiducials, which do not significantly affect the point-based

registration. With a high number of accurately localized surface fiducials, the least squares fit does not appear to be very sensitive to a small number of high error points. Therefore, it appears the TRE is lower because the internal fiducials are localized from the O-arm scans and are not affected by the conoscopic texture distortion.

While the TRE and FRE are affected by both texture error, localization error, and any non-rigid deformation that occurs between scans, the amount of non-rigid deformation observed is quite low. The mean non-rigid deformation observed was 0.5 mm, with a max of 2.4 mm.

Surface-based registration accuracy comparison

The accuracy of the ICP registration, which does not utilize texture information, is much less accurate than the texture-utilizing point-based registration.   While these results are not unexpected, they just underscore the importance of having the texture information available for registration. Without additional texture information, the lack distinctive geometric features on the kidney surface make it difficult for a pure surface-based registration to perform well.

This analysis establishes a best-case baseline for the point-based registration using texture landmarks. However, in future work, an additional comparison could be done using clinically realistic fiducials, whether marks applied to the surface using a non-toxic surgical marker or fiducials attached using a clinically safe adhesive.

Non-rigid deformation

While some previous work (described in Chapter 5) has suggested non-rigid deformation between 3-6 mm caused by fluid loss due to incisions, this work suggests that there is little deformation in the intact in-vivo kidney. Therefore, while non-rigid deformation correction may be important in other organs such as the liver, it may not be necessary in guidance systems for partial nephrectomy if the navigation is done before clamping.

Future work

While the accuracy for this method in-vivo in laparoscopic conditions are quite promising, future work remains before it could become practical clinically. First, in these experiments the conoscope was scanned across the kidney manually. While this allows the operator control over the surface targeted, manipulating the conoscope is somewhat difficult in a laparoscopic environment, and the scan line spacing and speed are not consistent. Two possible ways of improving ease of use are (1) decreasing the size of the conoscope or (2) automating the scanning process.

While decreasing the size of the conoscope would make the manual scanning process more convenient, it does not address the issue of line spacing and speed. Previous surface-based registration results using a manually scanned kidney phantom showed a mean TRE of 3mm and a max of 6mm [1]. If that surface-based error range or the texture registration error reported here is acceptable, then manual scanning with a smaller conoscope may be a viable solution to improve ease of scanning.

However, if the scanning process could be mechanically automated, it would not only make the scanning more convenient, but could potentially increase the accuracy due to more regular scan lines and speeds. An additional method would be necessary to segment the targeted surface from the background, but the texture map could be used for this segmentation.

Second, although surface fiducials were attached to the kidney in these experiments, we visualize a system that does not need them. In the future, a tracked object inserted into the inssuflated abdomen could be used to register the image to optically tracked space. The object could contain small beads in a known geometry, which could be localized in the O-arm image and registered to their locations in optically tracked space. Therefore the image to conoscopic space registration would not need the radio-opaque surface fiducials, as were used in this experiment. Instead, a non-toxic surgical marker could be used to place marks on the kidney that could be used to register the conoscopic scans after movement. In addition, an automated method of detecting surface fiducials from the texture could be developed.

Finally, while no pre-operative images were used in these experiments; future work could explore registering pre-operative images to the 3D fluoroscopic scan. Alternatively, the 3D fluoroscopic scan has the potential to be directly used for navigation if the scan were taken with intra-operative contrast agent. With contrast, the tumor and vessels would be visible for navigational purposes.

We envision the final clinical workflow to involve the following: (1) After the surgeon has isolated the kidney from its surrounding fascia and peri-renal fat, and immediately before any robot is moved into place, an initial tracked O-arm scan will be taken. (2) After the O-arm scan, the robot will be moved into place and the conoscope attached to a robotic manipulator. (3) The conoscopic scan will be taken (possibly automatically). In our experiments, without automation, the total scanning time was under 60 seconds. (4) After any kidney movement, additional conoscopic scans will be taken whenever the surgeon requires navigation.

While incorporating a tracked O-arm scan increases the time of surgery and radiation exposure, future work should asses those disadvantages against the benefits of navigation. In the past, other technological advances have had such great benefit as to outweigh similar disadvantages. For instance, the increasing popularity of robot-assisted laparoscopic nephrectomy is an example of a technological improvement whose benefits in some cases outweigh the increased time and cost of surgery.

While the previous issues deal with our vision for how the intra-operative conoscopic system could be used clinically, a few minor improvements could be made as well. One minor issue to address involves the conoscopic beam focus. In laparoscopic cases, the focus and range of the conoscope needs to accommodate the distance between the insufflated abdominal wall and the kidney. Currently, the focus of the conoscope is approximately 250 mm from the lens, and the range is about 200-300mm. In the pig, we found the conoscopic range to be at the lower limit of the range needed. Ideally, a longer focus would be more convenient, and in humans, an even longer range would probably be needed. Using a different lens on the conoscope would allow us to change the focus.

Finally, improvements could be made to the conoscopic attachment, which is inserted through the trocar port. It is important that these parts be made sterilizable and air-tight, so that the gas used to inssuflate the kidney does not escape through the trocar port.

Conclusion

In conclusion, we have shown the feasibility of an intra-operative registration method that can be used minimally invasively to correct for kidney movement.   This method uses an initial 3D fluoroscopic scan and successive textured conoscopic scans, from which features are localized and registered. We have shown the accuracy of this method in live, anesthetized pigs under laparoscopic conditions. The mean and maximum TRE were 0.6 mm and 2.0 mm, respectively, for 4 kidneys and 35 scans.

This method was shown to successfully account for kidney motion during mimimally invasive surgery, which is important for the abdominal organs that do not have proximal rigid bone structures by which to register. In addition, the conoscopic scans allow for registration after movement without additional O-arm scans and excessive radiation exposure. While there are several improvements that could be made, we believe this is a promising method that could enable minimally invasive guidance for kidney surgery.

References

[1]   Burgner, J., Simpson, A. L., Fitzpatrick, J. M., Lathrop, R. A., Herrell, S. D., Miga, M. I., and Webster, R. J. III, Conoscopic Holography for Intraoperative Digitization: Characterization and Application for Registration. (Submitted to International Journal of Medical Robotics and Computer Assisted Surgery, Dec. 2011.)

[2]   Pollak, J.S., & White, R. I. (2001). The Use of Cyanoacrylate Adhesives in Peripheral Embolization, *Journal of Vascular and Interventional Radiology,* 12(8): 907-913.

[3]   Trott, A. T. (1997). Cyanoacrylate Tissue Adhesives. *Journal of the American Medical Associations,* 277(19): 1559-1560.

[4]   Reece, T. B., Maxey, T. S., Kron, I. L. (2001). A Prospectus on Tissue Adhesives, *American Journal of Surgery*, 182(2): S40-S44.

[5] Simpson, A.L., Burgner J., Glisson, C. L., Pheiffer, T.S., Herrell, S.D., Webster, R. J. III, Miga, M. I. A Comparison Study of Contact and Non-Contact Surface Acquisition Methods with Application to Image-Guided Interventions. (Submitted to IEEE Transactions on Biomedical Engineering, Nov. 2011)

[6] Simpson, A. L., Burgner, J., Chen, I., Pheiffer, T. S., Sun, K., Thompson, R.J., Webster, R. J. III, Miga, M. I. (2012) Intraoperative Brain Tumor Resection Cavity Characterization with Conoscopic Holography, SPIE Medical Imaging, Feb. 4-9, San Diego, CA.

[7] Becker, F., et al., *Elective nephron sparing surgery should become standard treatment for small unilateral renal cell carcinoma: Long-term survival data of 216 patients.* Eur Urol, 2006. **49**(2): p. 308-13.

[8] Dunn, M.D., et al., *Laparoscopic versus open radical nephrectomy: a 9-year experience.* J Urol, 2000. **164**(4): p. 1153-9.

[9] Benway, B.M. and S.B. Bhayani, *Robot-assisted partial nephrectomy: evolution and recent advances.* Curr Opin Urol. **20**(2): p. 119-24.

[10] Scoll, B.J., et al., *Robot-assisted partial nephrectomy: a large single-institutional experience.* Urology. **75**(6): p. 1328-34.

[11] Kos, S., et al., *MR-guided endovascular interventions: a comprehensive review on techniques and applications.* European Radiology, 2008. **18**(4): p. 645-657.

[12] Peters, T. and K. Cleary, eds. *Image-Guided Interventions*. 2008, Springer: New York. 557.

[13] Ding, S., et al., *Semiautomatic registration of pre- and postbrain tumor resection laser range data: method and validation.* IEEE Trans Biomed Eng, 2009. **56**(3): p. 770-80.

[14] Dumpuri, P., et al., *Model-updated image-guided liver surgery: preliminary results using surface characterization.* Prog Biophys Mol Biol. **103**(2-3): p. 197-207.

[15] Clements, L.W., et al., *Robust surface registration using salient anatomical features for image-guided liver surgery: algorithm and validation.* Med Phys, 2008. **35**(6): p. 2528-40.

[16] Sirat, G.Y., *Conoscopic Holography .1. Basic Principles and Physical Basis.* Journal of the Optical Society of America a-Optics Image Science and Vision, 1992. **9**(1): p. 70-83.

[17]   Sirat, G.Y. and D. Psaltis, *Conoscopic Holograms.* Optics Communications, 1988. **65**(4): p. 243-249.

CHAPTER 5

NON-RIGID DEFORMATION OF THE KIDNEY DURING SURGERY

Portions of this chapter appeared in the *Proc. Of SPIE*: Ong, R. E., Glisson, C. L., Herrell, S. D., et al. (2009). A deformation model for non-rigid registration of the kidney, *Proceedings of SPIE*, 7261:72613A.

Introduction

The American Cancer Society has estimated that over 54,000 new cases of renal cancer will be diagnosed and over 13,000 people will die of the disease in 2008 [1].   Surgery is usually the recommend treatment if the renal tumors are found before metastasis. Partial nephrectomies, in which only a portion of the kidney is removed, are usually recommended over full nephrectomies for small renal tumors. Recent studies [2, 3] have found that patients who undergo partial nephrectomies have about the same tumor re-occurrence and long-term survival rates as those who undergo radical nephrectomies; however, partial nephrectomy patients have the advantage of retaining greater renal function.

One challenge surgeons face during partial nephrectomies is the location of sub-surface tumor margins, small tumors deep inside the kidney, blood vessels, and other structures that may not be visible from the kidney surface. To facilitate the location and removal of tumors during partial nephrectomies, an image-guided surgery system may be helpful. By providing the surgeon a navigational aid, this system would ideally allow the surgeon to spare more healthy nephrons while still obtaining a clear tumor margin and avoiding critical vessels. Image-guided renal systems are currently being developed that utilize pre-operative and intra-operative imaging to provide an interactive display of the kidney. These systems generally require the registration of pre-operative and intra-operative images to the physical kidney and the tracking of surgical tools. Much work has been done previously to develop image-guided surgery systems for the brain, liver, and other organs [4-6].

Ideally, an image-guided renal surgery system would not only account for changes in kidney position and orientation by performing a rigid alignment, but also for changes in kidney shape that occur during surgery. This non-rigid deformation may be caused by external forces applied to the kidney (e.g. by surgical tools, retractors, or laparoscopic insufflation), by physiological changes, or by other surgical conditions. One surgical condition that may cause non-rigid kidney deformation is the clamping of the renal vessels. During partial nephrectomies, the renal artery and vein are often clamped, causing a loss of perfusion. The subsequent cutting of the kidney during surgery causes blood and fluid loss, which decreases intrarenal pressure, inducing a loss of turgor and general shrinkage of the kidney. The extent of the deformation caused by intrarenal pressure decreases and whether it can be corrected for in an image-guided surgical system is not well known.

In our previous work [7], we found that resected human kidneys experienced a mean shift of about 3 mm when subjected to clamping and unclamping; however, the decrease in perfusion pressure and an incision to the parenchyma was not controlled.

In this work, we attempt to measure and predict the deformation that occurs when a kidney under a controlled renal arterial pressure is subject to a parenchymal incision. To predict the deformation, we investigate using a spline interpolation to estimate the displacements tracked by the surface fiducials. While this method used CT scans to track surface fiducials, in the future feature tracking in conoscopic textured surfaces could be used to find these displacements. The ultimate goal of this prediction method is to correct for the intra-operative kidney deformation in an image-guided renal surgery system.

Methods

Experiments

To track the kidney deformation that occurs when the renal vessels are clamped and a parenchymal incision is made, the following procedure was followed:

1. Three anesthesized pigs were heparinized to prevent blood clots and euthanized. The six porcine kidneys were then resected.

2. Between 10-20 glass bead fiducials 2 mm in diameter were attached to each kidney surface, and the kidneys were fixed to their enclosing containers in order to eliminate any rigid motion.

3. The kidneys were perfused with saline at a renal arterial pressure of 100mmHg, a physiologically reasonable pressure. To this end, the renal artery and vein of the resected porcine kidneys were cannulated with tubing 1-3mm in diameter, and the tubing was sutured to the vessels to keep it from slipping out. The tubing was connected to 1000mL intravenous saline bags and primed before attachment to the renal vessels. The saline IV bags were hung 1.36 m above the kidney to induce a renal arterial pressure of 100mmHg. The saline was allowed to flow for a few minutes so that equilibrium could be reached.

4. The renal artery and vein were clamped.

5. A pre-deformation CT image of each kidney was taken (90 KeV, 300 mAs, 0.8 mm slice thickness). The kidney container was clamped to the CT table to eliminate any rigid motion.

6. A scalpel whose tip was tracked by a Polaris Spectra (Northern Digital Inc., Ontario, Canada) infrared tracking device was used to make an incision in the renal parenchyma. Blood and fluid were allowed to drain from the incision site. A Polaris target attached to the handle of the scalpel (Figure 1), and a prior calibration allowed the scalpel tip to be localized. To enable the registration of the scalpel coordinates to the kidney/CT image space, 6-8 glass bead fiducials 5mm in diameter were glued to the kidney container were localized using a Polaris probe.

7. A post-deformation CT image of the kidney was taken. As the kidney container was clamped to the CT table, the post- and pre-deformation images should be in the same coordinate space and no rigid registration should be necessary.

To measure the amount of deformation, the 2mm glass fiducials were localized in the pre- and post-deformation CT images by calculating the intensity-based centroids. The mean shift at the surface fiducials was then calculated for the six kidneys. The tracked scalpel was

rigidly registered to the CT image space using the six glass fiducials glued to the kidney container.

Figure 1. Scalpel with Polaris target attached to handle, used to track an incision made to the renal parenchyma.

Figure 2. Porcine kidney with glass bead fiducials attached to the surface to track deformation. The kidney was perfused with saline and cut with tracked scalpel.

Spline Interpolation

In order to predict the deformation caused by an incision, we investigated using thin-plate splines [10]. This method calculates the displacements tracked at the surface fiducials and interpolates them to the entire kidney volume. In this method, the kidney surface before the incision was split along a surface defined by the tracked scalpel (Figure 3). The fiducial displacements on each side of the incision were then interpolated to the kidney volume on that side of the incision.

The following thin plate spline equations are used to interpolate the displacements at the surface fiducials:

$$P_{target} = A\,P_{Source} + D + \sum_{i=1}^{length(P_{source})} W_i\,\|P_{source} - P_{source\,i}\|^2 \ln\left(\|P_{source} - P_{source\,i}\|\right)$$

[Eq. 1]

where P_{source} and P_{target} are the source and target surface fiducial positions; W_i are the weights describing the non-linear portion of the spline, **A** is a 3x3 affine transformation, and **D** is a 3x1 translation vector. This equation is solved for the weights W_i, **A**, and **D**.

The displacements are then interpolated to the volume mesh nodes **V**target and **V**source:

$$V_{target} = A\,V_{Source} + D + \sum_{i=1}^{length(P_{source})} W_i\,\|V_{source} - P_{source\,i}\|^2 \ln\left(\|V_{source} - P_{source\,i}\|\right)$$

[Eq. 2]
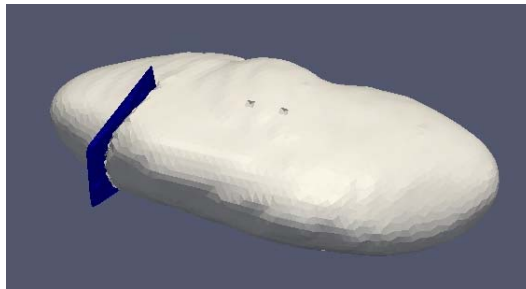
Figure 3a. Pre-incision kidney surface (white) shown with tracked scalpel plane (blue) that was used to split the mesh.
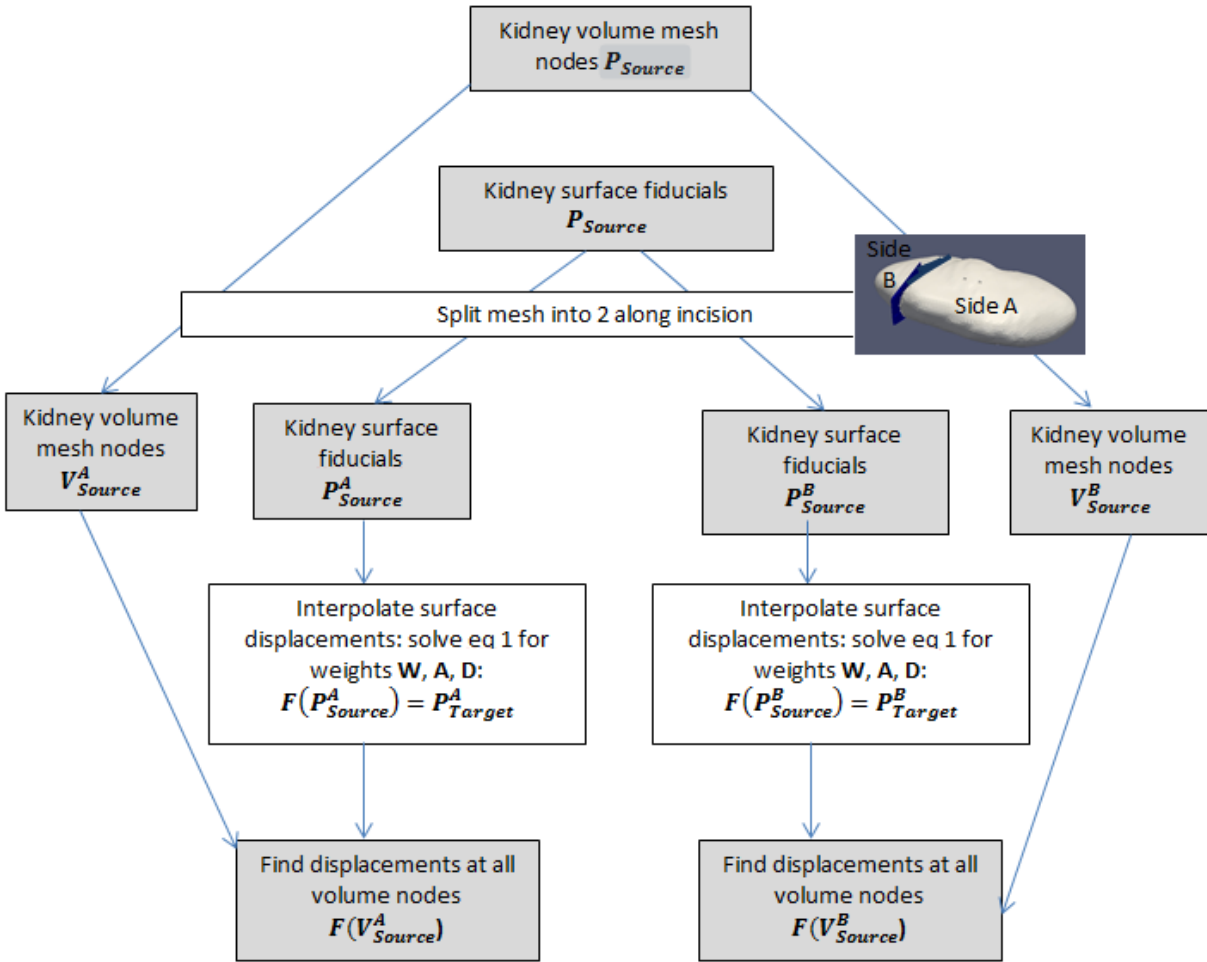
Figure 3b. Diagram illustrating the spline interpolation process.

The accuracy of this method was evaluated for the 6 pig kidneys described above, for different numbers of control points across the kidney. Random combinations of surface fiducials were picked to be the control points, while the remaining fiducials were used as targets to calculate TRE. The numbers of control points tested were 5, 10, 15, 20, 25, and 30, while the maximum number of fiducials was 32. Because the number of combinations of fiducials is so many, for each number of control points, 100 random samples were taken.

Certain constraints were used when picking the fiducials to be used as the spline control points. The fiducials had to cover at least half the length of the kidney, and the base fiducials

were not included. At the base fiducials, the displacements were set to 0 to simulate the fixed bottom kidney surface in the experiment.

Results

Deformation Measurement

The amount of deformation that occurred when six pig kidneys were perfused at 100mmHg, clamped, and then cut with a scalpel is shown in Table 1. The displacements measured at the surface fiducials localized in the pre- and post-deformation images was found to be between 3-6 mm. The mean deformation for all six kidneys was 4.4 mm. The magnitudes of the displacements as distributed across the surface of the kidney can be seen in Figure 4. Here we observed that the displacement magnitudes in general decrease with increased distance from the incision.

Table 1. Amount of deformation that occurred when six pig kidneys were perfused at 100mmHg, clamped, and then cut with a scalpel. Displacement was tracked using glass fiducials, localized from pre- and post-deformation CT images, and the mean shift at these surface fiducials was then calculated.

	Displacement at surface fiducials (mm)		
Kidney	Mean	Std dev	Max
1	4.7	2.2	9.2
2	3.4	2.0	7.4
3	6.7	2.4	11.4
4	4.5	2.2	7.2
5	3.8	1.7	6.1
6	3.4	1.8	5.7
Mean	4.4		
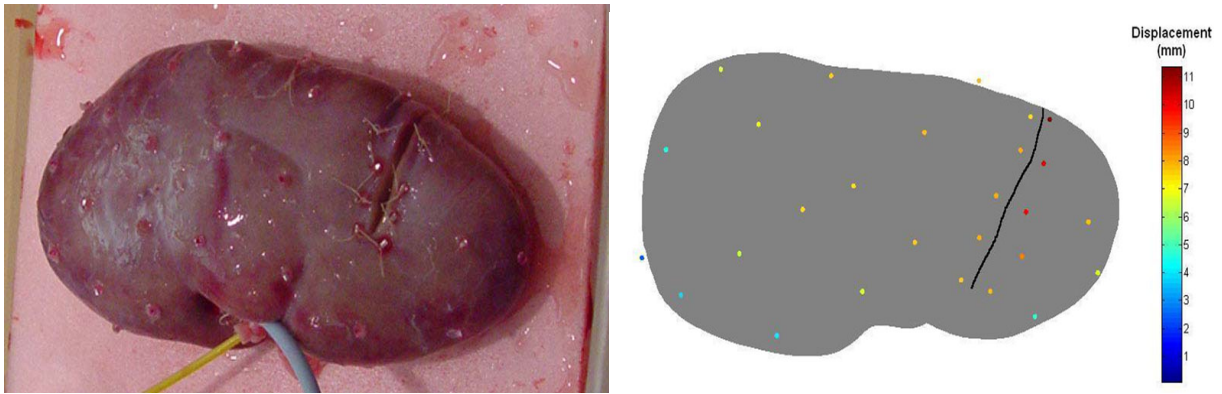
Figure 4. Left: Photograph of pig kidney 6 post-incision. Fiducials attached to the surface can be seen. Right: Fiducial locations color-coded by absolute distance change.

Spline interpolation

Some representative visual results of the spline interpolation are shown for pig 1 (using 30 control points) in Figures 5 and 6. The split, spline-interpolated surface matches up quite well visually with the gold standard post-incision CT surface. As the closest distances show, there is low error long most of the kidney surface, with the exception of a few places near the incision and towards the bottom of the kidney.

The quantitative results for all 5 kidneys, including the TRE and closest point distances, are shown in Table 2. The graph in Figure 7 shows the TRE grouped by numbers of control points, while Figure 6 shows the error distributions.
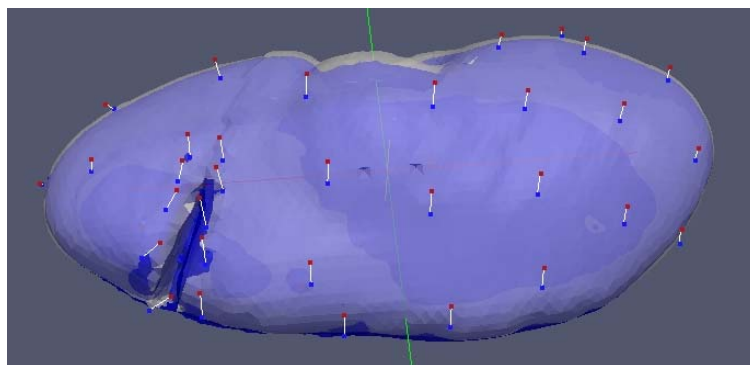
Figure 5. Spline-interpolated surface (transparent white, pig 1, 30 control points) overlaid on gold standard post-incision CT surface (blue). The white lines represent the displacements tracked at the fiducials.
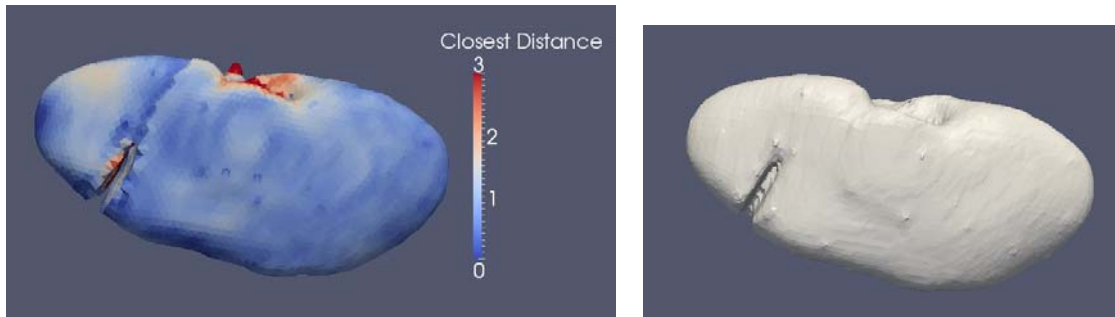
Figure 6. Closest distances between spline-interpolated kidney surface (left: pig 1, 30 control points) and gold standard post-incision CT surface.

Table 2. Accuracy of spline interpolation for different numbers of fiducial control points, over 100 random combinations of control points. The TRE and closest distances are reported. (Pig 5 had corrupted tracking data, so it could not be processed.)

	Nbr of Ctrl Pts	TRE over 100 trials (mm)					Closest distances (mm)			
		Mean	Std	Min	Max	Median	Mean	Std	Min	Max
Pig1	5	2.3	2.0	0.0	9.2	1.7	1.3	1.1	0.0	7.8
	10	1.6	1.6	0.0	9.2	1.0	1.0	0.9	0.0	7.8
	15	1.3	1.3	0.0	7.7	0.8	1.0	0.9	0.0	7.3
	20	1.1	1.2	0.1	7.4	0.7	0.9	0.9	0.0	7.3
	25	1.0	1.1	0.1	6.2	0.7	0.9	0.9	0.0	7.3
	30	0.9	0.9	0.1	5.7	0.5	0.9	0.8	0.0	7.3
Pig2	5	2.0	1.6	0.1	7.3	1.6	1.0	1.2	0.0	8.7
	10	1.4	1.1	0.1	7.1	1.0	0.8	1.0	0.0	8.7
	15	1.1	0.8	0.1	4.3	0.9	0.7	1.0	0.0	8.7
	20	0.9	0.7	0.1	2.9	0.8	0.7	1.0	0.0	8.6
Pig3	5	2.9	2.1	0.1	11.4	2.4	1.4	1.6	0.0	11.5
	10	2.0	1.6	0.0	9.9	1.5	1.2	1.5	0.0	11.5
	15	1.6	1.3	0.1	9.4	1.1	1.1	1.5	0.0	11.5
	20	1.3	1.1	0.1	6.4	1.0	1.0	1.5	0.0	11.5
Pig4	5	2.1	1.4	0.1	7.2	1.7	1.1	1.0	0.0	7.1
	10	1.3	0.9	0.0	6.1	1.2	0.9	0.8	0.0	5.8
	15	1.0	0.7	0.0	5.0	1.0	0.7	0.8	0.0	5.8
	20	0.9	0.5	0.0	2.4	0.8	0.7	0.7	0.0	5.8
Pig6	5	2.0	1.3	0.1	5.6	1.7	1.2	1.5	0.0	13.4
	10	1.6	1.2	0.1	5.1	1.3	1.1	1.5	0.0	13.3
	15	1.5	1.1	0.1	4.7	1.3	1.1	1.5	0.0	13.2
	20	1.4	1.1	0.1	4.3	1.1	1.1	1.5	0.0	13.2
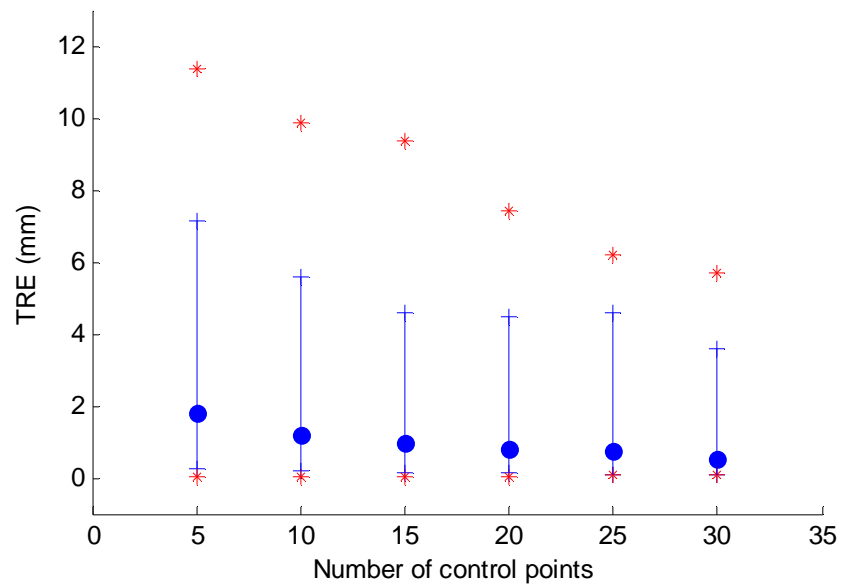
Figure 7. Accuracy of spline interpolation for different numbers of control points (for all 5 kidneys and 100 trials). The blue dots represent the median TRE, the blue bars the 5th and 95th percentiles, and the red stars the minimum and maximum TRE.
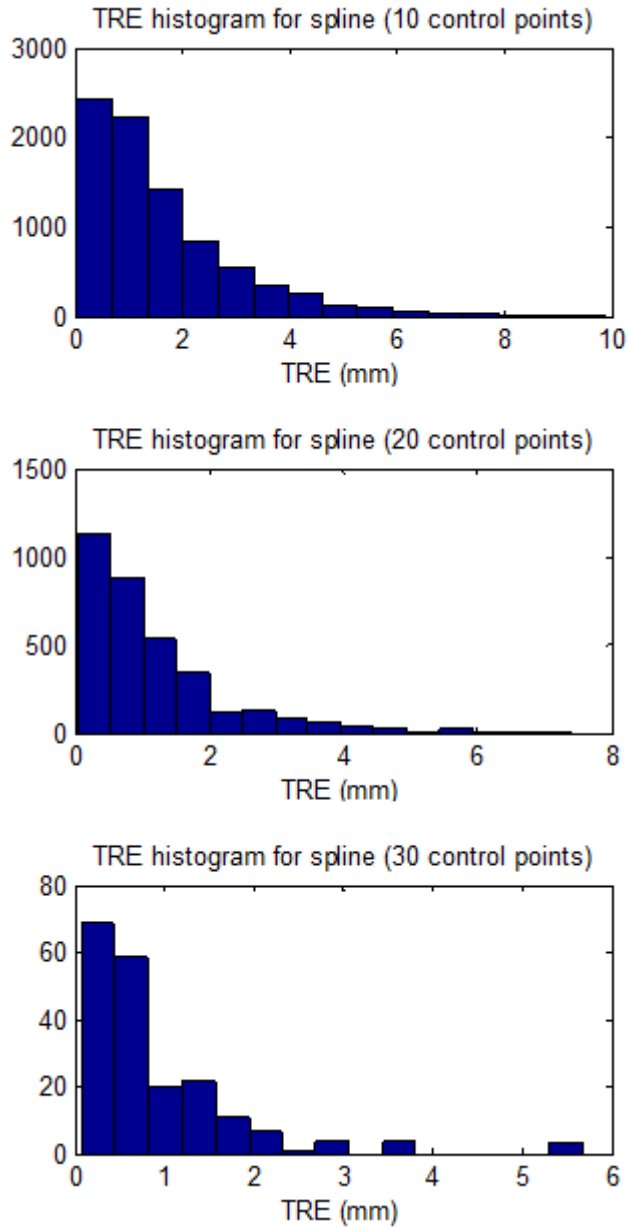
Figure 8. Error histograms for the spline interpolations for different numbers of control points (for all 5 kidneys and 100 trials).

Discussion

In this work, we have measured the non-rigid deformation in 6 clamped porcine kidneys caused by an incision and subsequent fluid loss. While previous work in human cases (Chapter 2) and in-vivo pigs (Chapter 4) indicates that little non-rigid deformation occurs prior to incision, this work shows that mean displacements of between 3-7 mm can occur after an incision.

In addition to measuring the extent of deformation, we have attempted to predict the displacements using thin-plate spline interpolation. In this method, the pre-incision kidney mesh is split along a surface described by the tracked scalpel, and the displacements at the tracked fiducials are interpolated to the entire kidney. The results for using 30 surface fiducials as spline control points show a mean TRE of 0.9 mm.

Future work

While the CT scanning method used to track the fiducials in this experiment is not practical clinically, the spline interpolation method described here could use features tracked from conoscopic textured surfaces instead. In chapter 4 of this work, we showed that conoscopic textured surfaces obtained intra-operatively could be used to track features on the kidney surface. While that work only dealt with rigid registrations and the non-punctured kidney, it would be possible to extend that method to account for non-rigid deformation due to incisions. This could be done by calculating displacements from features localized in pre- and post-incision conoscopic scans. These displacements would be then be interpolated to the entire kidney volume as described in this paper.

In addition, we would like to explore using the Laplace method to interpolate displacements instead of thin-plate splines, as the Laplace method could have several advantages. First, as the displacements on either side of the incision would not have to be interpolated separately, the discontinuity along the incision plane would be eliminated. The pre-processing of the mesh would also be simplified.
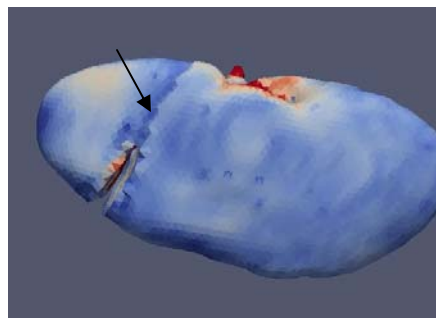
Figure 9. Discontinuity along incision plane due to the separate interpolations done on either side of the incision plane.

Conclusion

In this work we have measured the extent of non-rigid deformation that occurs because of fluid loss due to an incision in the kidney. We have also investigated a spline-based interpolation of the fiducial-tracked displacements to predict non-rigid deformation. We believe that with further work, including a possible investigation of Laplace's method for interpolation, an interpolation method could be used in conjunction with conoscopic texture feature-tracking to correct for non-rigid deformation for image guidance in the kidney.

Appendix

In addition to the spline interpolation, a linear elastic (isotropic and anisotropic) model was also used to predict the kidney deformation. These results were not included in the body of the paper as the models were only run on one kidney, and the results were not very accurate.

Methods

The linear elastic model and anisotropic linear elastic model were used to predict the displacements for the third kidney described in the main methods section of this paper. The boundary conditions were set as follows: the bottom surface and hilum area of the kidney were fixed, a type 2 surface force of 70 Pa in the outward normal direction was applied at the incision, and a type 2 surface force of 1000 Pa was applied in the direction of gravity to simulate the loss of turgor due to loss of intrarenal pressure. For the anisotropic model, the properties shown in Table 1 were used. The isotropic model parameters were set as follows: Young's modulus E=8300 Pa, Poisson's ratio Nu=0.45. All three models were solved in three Cartesian dimensions using the Galerkin finite element method and Lagrange polynomial weighting functions.

The directions of the renal tubules, from which the anisotropic directions were obtained, were generated by the following method: the approximate medial axis was found, and for each mesh node, the closest point on the medial axis was found. Thus the shortest vectors connecting each mesh node with the medial axis were found and assigned as the directions of anisotropy. See Figure 10 for an illustration of the medial axis and generated renal tubule directions.
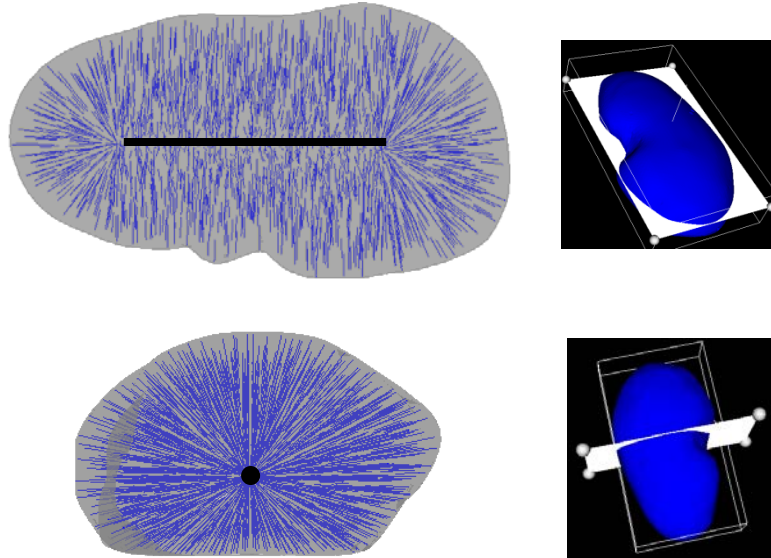
Figure 10. Two orthogonal views of pig kidney, with simulated renal tubules displayed by blue vectors. The thick black line indicates the medial axis from which the renal tubules were generated.

Table 3. Anisotropic linear elastic model parameters: Young's modulus (E) and Poisson's ratio (Nu) for longitudinal (L) and transverse (T) directions and shear modulus (G).

E_L (Pa)	E_T (Pa)	Nu_L	Nu_T	G
10000	5000	0.4	0.2	2083.33

Results

The general pattern of deformation predicted by the anisotropic linear elastic model is shown in Figure 11, which displays the signed closest distance between the pre- and post-deformation meshes. A negative distance in this case indicates an area where the post-deformed mesh is located inside the pre-deformed mesh, and a positive distance where the post-deformed is outside the pre-deformed mesh. Here we see the model predicts a general "sinking in" of the kidney surface in the direction of gravity (indicated by the blue areas), and a small expansion along the lateral edges (indicated by the green). Figure 12 displays the model-predicted and true displacement vectors.

The TRE and magnitude error for two simulations is shown in Table 4. The anistropic linear elastic model performed the best, but only slightly better than the linear elastic model. The porous media model incorporating an anisotropic hydraulic conductivity tensor had much higher TRE and magnitude errors.

Table 4. TRE and magnitude error for linear elastic and anisotropic linear elastic models for kidney 3.

	TRE (mm)			Magitude error (mm)		
	Mean	Median	Max	Mean	Median	Max
Linear elastic model	3.4	3.3	6.5	1.6	1.6	5.3
Anisotropic linear elastic	3.2	3.0	6.2	1.6	1.2	4.9

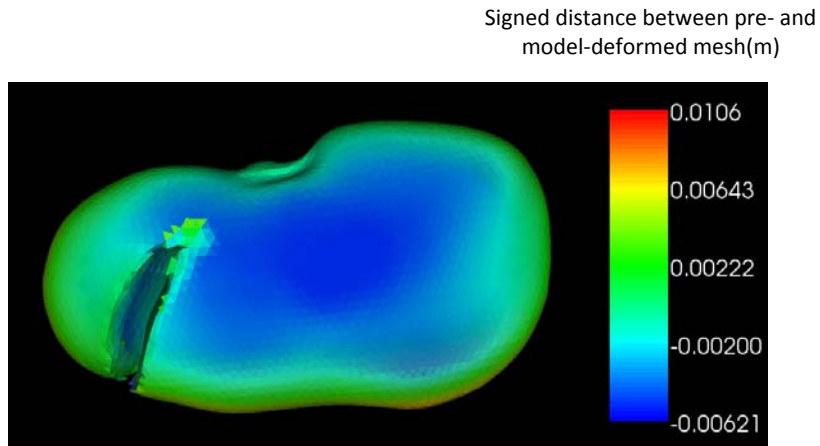Signed distance between pre- and model-deformed mesh(m)

Figure 11. Mesh deformed by anisotropic linear elastic model, where color represents the signed distance between the pre-deformation and model-deformed meshes for kidney 3. Negative distances represent where model-deformed mesh has "sunken in" and positive distances where the mesh has "expanded out."
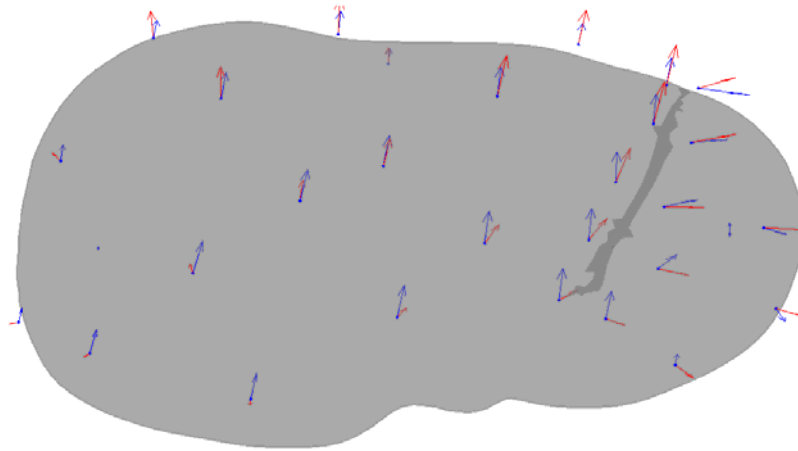
Figure 12. Pre-deformation mesh for kidney 3 with blue arrows representing true displacements and red arrows representing displacements predicted by the anisotropic linear elastic model.

References

[1] American Cancer Society. 2007. "Cancer Facts and Figures." www.cancer.org.

[2] Becker, F., Siemer, S., Humke, U., et al. "Elective nephron sparing surgery should become standard treatment for small unilateral renal cell carcinoma: Long-term survival data of 216 patients." Eur Urol. 49(2), 308-13 (2006).

[3] Lau, W.K., Blute, M.L., Weaver, A.L., Torres, V.E., Zincke, H. "Matched comparison of radical nephrectomy vs nephron-sparing surgery in patients with unilateral renal cell carcinoma and a normal contralateral kidney." Mayo Clin Proc. 75(12), 1236-42 (2000).

[4] Benincasa, A.B., Clements, L.W., Herrel, S.D., Chang, S.S., Cookson, M. S., Galloway R. L. "Feasibility study for image guided kidney surgery: assessment of required intraoperative surface for accurate image to physical space registrations." Proc. of SPIE 6141, 61411U (2006).

[5] Dumpuri, P., Thompson, R. C., Dawant, B. M., Cao, A., Miga, M. I. "An atlas-based method to compensate for brain shift: Preliminary results." Medical Image Analysis 11(2),128-145 (2007).

[6] Miga, M.I., Cash, D. M., Cao, Z., Galloway, R. L., Dawant, B., Chapman, W. C. "Intraoperative registration of the liver for image-guided surgery using laser range scanning and deformable models." Proc. of SPIE 5029, 350-359 (2003).

[7] Ong, R. E., Herrell, S. D., Miga, M. I., Galloway, R. L. "A kidney deformation model for use in non-rigid registration during image-guided surgery," Proc. of SPIE: Medical Imaging (2008).

[8] Farshad, M., Barbezat, M., Flueler, P., Schmidlin, F., Graber, P., Niederer, P. "Material characterization of the pig kidney in relation with the biomechanical analysis of renal trauma." J Biomech. 32(4), 417-425 (1999).

[9] Miller, K. "Constitutive modeling of abdominal organs." Journal of Biomechanics. 33, 367-373 (2000).

[10] Goshtasby, A. (1988). Registration of images with geometric distortions, IEEE Transactions on Medical Imaging, 26(1): 60-64.

CHAPTER 6

CONCLUSION AND FUTURE WORK

In this work, we have developed and evaluated a novel intra-operative registration method for minimally invasive kidney surgery. In order to do this, we first evaluated an intra-operative registration method using laser scanning methods in open clinical cases, as described in Chapter 2 and published in [1]. The results of this study showed the feasibility of using texture-mapped, laser-scanned surfaces to track features for intra-operative registration. While previous work had explored using the LRS for intra-operative registration in the brain and liver [6-8], this work represents the first time it had been evaluated in the kidney in human clinical cases.

Second, we extended the intra-operative laser scanning and registration methods described in Chapter 2 for minimally invasive surgery. To do this, we used a conoscopic laser, which is small enough to be used minimally invasively, to scan the kidney surface intra-operatively. Although conoscopic scanning had been investigated previously [9-11], the contribution of this work was to introduce a novel texture-mapping algorithm that enables intra-operative feature-tracking. This method is described and evaluated for accuracy in Chapter 3. The results of this study were promising and showed a mean texture error below 1 mm and maximum below 3.5mm for 10 cases.

Finally, we explored the feasibility of using the textured conoscopic surfaces for intra-operative registration in minimally invasive, in-vivo conditions in Chapter 4. The contribution of this work was to evaluate the accuracy of the novel conoscopic texturing algorithm with tracked 3D fluoroscopy. While the previous section evaluated the accuracy of the textured conoscopic surface in ex-vivo kidneys, this section evaluates a full registration method in-vivo in anesthetized swine under laparoscopic conditions. The point-based registration method used features localized from the conoscopic textured surfaces to align kidney surfaces after movement. The accuracy of the registration method was evaluated by calculating the TRE, which was shown to be 1mm or below for the 4 kidneys and 35 scans taken.

In addition, we have explored some causes of non-rigid kidney deformation in order to evaluate the need for deformation correction in image-guided systems. This work was described in Chapter 5 and published in [2] and [3]. Prior to this work, little had been known about the deformation of the kidney under surgical conditions. Previous work had been done to measure the stiffness of ex-vivo porcine kidneys [4-5], but there had not been any work on the deformation resulting from clamping and incision in a perfused kidney. The contribution of this work was to investigate the deformation caused by the loss of fluid due to an incision using perfused ex-vivo pig kidneys. The extent of the deformation was measured, and we found a mean displacement of 3-7 mm. In addition, we investigated using thin-plate splines to interpolate fiducial-tracked displacements to predict the deformation. This method could be used in conjuction with conoscopic texture scanning to track features and interpolate the displacements to the entire kidney.

In these studies, we found only small amounts of non-rigid deformation in the kidney prior to clamping, as measured by internal fiducials in four in-vivo pigs. Even after clamping of the renal vessels and icing of the kidney, we observed little deformation in the clinical cases as measured by surface fiducials. However, the number of cases was small and the deformation was only measured at the surface, so further studies are needed before a definitive conclusion can be made about the deformation after clamping.

While little deformation was found before clamping of the renal vessels, we have seen more significant deformation after incision and fluid loss, with mean deformations of 3-7 mm.

These findings indicate that if image guidance for the kidney is performed prior to clamping, non-rigid deformation correction may not be needed. However, after any incision causing fluid loss, significant deformation may occur and require correction.

Future work

Before the intra-operative registration methods presented here could be used clinically, work still remains. First, we would like to increase the ease at which the conoscope is scanned across the kidney. Currently, the conoscope is swept across the kidney manually, and this can be difficult in a laparoscopic environment. Either decreasing the conoscope size for the

purpose of manual scanning or mechanically automating the scanning could improve the ease of use. While manual scanning allows more control over the scanned area, automated scanning would increase the regularity of the scan line spacing and speed, potentially increasing accuracy.

Second, although surface fiducials were attached to the kidney in the conoscopic registration experiments, we visualize a system that does not need them. In the future, a tracked target inserted into the insufflated abdomen could be used to register the image to optically-tracked space. Therefore the image to conoscopic space registration would not need the radio-opaque surface fiducials. Instead, a non-toxic surgical marker could be used to place marks on the kidney that could be used to register the conoscopic scans after movement.

If these major improvements could be made and further accuracy studies performed, we believe intra-operative registration for minimally invasive kidney surgery may be feasible. If guidance is provided before clamping of the renal vessels and incision, the rigid registration method presented in Chapter 4 could be sufficient. Given that the range of reported TRE for the rigid registration is acceptable (mean TRE of 0.6mm, max 2.0mm), deformation correction may not be needed.

Finally, if guidance is needed after clamping or incision, further investigation into non-rigid deformation correction is needed. While the spline-based interpolation described in Chapter 5 is promising, especially if used in conjunction with the feature-tracking from conoscopic textured surfaces, more work needs to be done. In particular, the Laplace method of interpolation could be explored, and methods for dealing with fiducials that have disappeared after resection should be developed.

Developing intra-operative guidance for minimally invasive kidney surgery is an exciting challenge, and this work has made progress towards achieving that goal.

References

[1]   Ong, R.E., Glisson, C. L., Altamar, H., Viprakasit, D., Clark, P., Herrell, S.D., Galloway, R.L. (2010). Intraprocedural Registration for Image-Guided Kidney Surgery, *IEEE Transactions on Mechatronics*, 15(6): 847-852.

[2]   Ong, R. E., Glisson, C. L., Herrell, S. D., et al. (2009). A deformation model for non-rigid
        registration of the kidney, *Proceedings of SPIE* ,7261:72613A.

[3]   Ong, R. E., Herrell, S. D., Miga, M. I., Galloway, R. L. (2008). A kidney deformation
        model for use in non-rigid registration during image-guided surgery, *Proc. of SPIE:
        Medical Imaging*.

[4]   Farshad, M., Barbezat, M., Flueler, P., Schmidlin, F., Graber, P., Niederer, P. (1999)
        Material characterization of the pig kidney in relation with the biomechanical analysis of
        renal trauma, *J Biomech*. 32(4), 417-425.

[5]   Miller, K. (2000). Constitutive modeling of abdominal organs, *Journal of Biomechanics*.
        33:367-373.

[6]   Dumpuri, P., et al., *Model-updated image-guided liver surgery: preliminary results using
        surface characterization.* Prog Biophys Mol Biol. **103**(2-3): p. 197-207.

[7]   Clements, L.W., et al., *Robust surface registration using salient anatomical features for
        image-guided liver surgery: algorithm and validation.* Med Phys, 2008. **35**(6): p. 2528-40.

[8]   Ding, S., et al., *Semiautomatic registration of pre- and postbrain tumor resection laser
        range data: method and validation.* IEEE Trans Biomed Eng, 2009. **56**(3): p. 770-80.

[9]   Burgner, J., Simpson, A. L., Fitzpatrick, J. M., Lathrop, R. A., Herrell, S. D., Miga, M. I., and
        Webster, R. J. III, Conoscopic Holography for Intraoperative Digitization:
        Characterization and Application for Registration. (Submitted to International Journal of
        Medical Robotics and Computer Assisted Surgery, Dec. 2011.)

[10]   Simpson, A.L., Burgner J., Glisson, C. L., Pheiffer, T.S., Herrell, S.D., Webster, R. J. III,
        Miga, M. I. A Comparison Study of Contact and Non-Contact Surface Acquisition
        Methods with Application to Image-Guided Interventions. (Submitted to IEEE
        Transactions on Biomedical Engineering, Nov. 2011.)

[11]   Simpson, A. L., Burgner, J., Chen, I., Pheiffer, T. S., Sun, K., Thompson, R.J., Webster, R. J.
        III, Miga, M. I. (2012) Intraoperative Brain Tumor Resection Cavity Characterization
        with Conoscopic Holography, SPIE Medical Imaging, Feb. 4-9, San Diego, CA.